Relating Critical and Limiting Fluxes to Metastable and Long-term Stable Fluxes in Colloidal Membrane Filtration Through Collision-Attachment Theory

Junxia Liu [1], Wei Fu [1], Xuri Yu [1], Haiyan Yang [2, *], Dongsheng Zhao[3], Zhihong Wang[1], Lin Wang [4, **], Xianhui Li [5], Chuyang Y. Tang [6]

[1] School of Civil and Transportation Engineering, Guangdong University of Technology, Guangzhou 510006, China

[2] SCNU Environmental Research Institute, Guangdong Provincial Key Laboratory of Chemical Pollution and Environmental Safety & MOE Key Laboratory of Theoretical Chemistry of Environment, School of Environment, South China Normal University, Guangzhou 510006, China

[3] College of Civil Engineering and Architecture, Nanyang Normal University, Nanyang 473061, China

[4] School of Municipal and Environmental Engineering, Shandong Jianzhu University, Jinan 250101, China

[5] Key Laboratory for City Cluster Environmental Safety and Green Development of the Ministry of Education, School of Ecology, Environment and Resources, Guangdong University of Technology, Guangzhou, 510006, China

[6] Department of Civil Engineering, The University of Hong Kong, Pokfulam, Hong Kong

Corresponding Author

* haiyan.yang@m.scnu.edu.cn (H. Yang), ** lynn04@126.com (L. Wang)

Abstract

In membrane technology for water/wastewater treatment, the concepts of critical flux (J_C) and limiting flux (J_L) suggest the existence of a threshold flux below which no fouling occurs. However, their important roles on stable flux duration have not been sufficiently understood. This work adopts a collision-attachment approach to clarify the relationship of J_C, J_L to metastable (i.e., short-term stable) and long-term stable fluxes based on their dependence on initial flux (J_0), foulant-clean-membrane energy barrier ($E_{f\text{-}m}$), and foulant-fouled-membrane energy barrier ($E_{f\text{-}f}$). When J_0 is below J_L, water flux remains stable over a long time even for the case of J_0 over J_C, thanks to the strongly repulsive $E_{f\text{-}f}$. At $J_0 > J_L$ and $J_0 > J_C$, the water flux is unstable at the beginning of filtration, and the flux ultimately decreases to J_L as the long-term stable flux. Under the condition of $J_L < J_0 \leq J_C$, an initial metastable flux appears owing to the high $E_{f\text{-}m}$, with longer metastable period observed at lower J_0 and for more hydrophilic/charged membrane or colloids. Nevertheless, rapid flux decline occurs subsequently due to the energy barrier shifting to weak $E_{f\text{-}f}$, and the water flux eventually degenerates to J_L in long-term fouling duration. Our results provide significant guidelines for fouling control strategies with respect to membrane design, feedwater pretreatment, and operational optimization.

Keywords

Critical flux; Limiting flux; Metastable flux; Long-term stable flux; Collision attachment theory

1 Introduction

Owing to the merits of excellent performance, small footprint, and low energy consumption, nanofiltration (NF) and reverse osmosis (RO) have attracted great attention in advanced water/wastewater treatment field (Khanzada et al. 2020, Osorio et al. 2022, Su et al. 2021). However, membrane fouling, particularly colloidal fouling is consistently the bottleneck that restricts its wide application (Shannon et al. 2008, Tang et al. 2011, Zhang et al. 2016). Generally speaking, colloidal fouling is highly affected by membrane properties (i.e., charge (Wang et al. 2019), hydrophobicity (Shan et al. 2016) and roughness (Hoek et al. 2003)), feed characteristics (including colloidal charge (Boussu et al. 2007), colloidal hydrophobicity (Wang et al. 2016), and solution chemistry (Chen et al. 2017)), and operational conditions (e.g., permeate flux (Wang and Tang 2011b) and crossflow velocity (Tang et al. 2011)).

Among all the above factors, permeate flux is a particularly interesting parameter. As an important landmark, the theory of critical flux was proposed by Field et al. (1995) and Bacchin et al. (1995) in 1995, who stated that there existed a critical flux below which little fouling happened; above it fouling was observed. The critical flux is strongly dependent on colloid-membrane interaction (Tang et al. 2011, Xie et al. 2021). For instance, elevated critical flux was observed for more hydrophilic membrane, thanks to the strengthened hydration repulsion of foulant-clean-membrane (F-M)

(Etemadi et al. 2020, Xie et al. 2021). Another equally important concept is the limiting flux, which represents the maximum stationary flux achieved when increasing pressure for a given solution (Aimar and Field 1992, Porter 1972, Tang and Leckie 2007). In contrast to the critical flux corresponding to the fouling triggering on start-up, the limiting flux scales a maximum stable flux after fouling saturation. Tang and Leckie (2007) observed that all the fluxes curves above a threshold eventually collapsed to an identical pseudo stable value (i.e., limiting flux), whereas flux loss was negligible for operating flux below the limiting value. The limiting flux is significantly influenced by solution chemistry. For typical organic colloids (e.g., humic acid and protein), high limiting flux was observed at high pH or low ionic strength owing to the enhanced electrostatic repulsion of foulant-fouled-membrane (F-F) (Tang et al. 2009, Tang and Leckie 2007, Wang and Tang 2011b). In past few decades, both the critical and limiting fluxes have been applied as effective strategies for fouling control (Bacchin et al. 2006, Field and Pearce 2011, Lan et al. 2017, Tang et al. 2011).

According to the concept of critical /limiting flux, membrane flux can remain stable over a long time when the initial flux below a threshold value (Bacchin et al. 2006, Tang et al. 2011). However, metastable flux was experimentally observed recently that flux curves under constant pressure began to substantially decline after experiencing hours' or days' initial metastable period (Shan et al. 2016, Wang et al. 2016, Wang et al. 2019). Obviously, such "metastable flux" does not conform to the critical or limiting flux strictly. Nevertheless, it is greatly promising as a novel effective antifouling strategy by extending the metastable period. Thus, one may ask: "Why does the metastable flux drop unexpectedly? How can we extend the metastable period effectively? What are the relationships between critical flux (or limiting flux) and short-term and long-term stable fluxes?" All these doubts need to be carefully clarified for effective fouling control. Recently, Liu et al. (2020) expounded that the initial metastable flux appeared at high F-M but low F-F interaction. Since critical flux and limiting flux are also greatly affected by colloid-surface interaction (Liu et al. 2020, Tang and Leckie 2007), a comprehensive examination of F-M and F-F effects on colloidal stability is essential for clarifying the relations of critical and limiting fluxes to stable flux duration. Furthermore, as the colloid-membrane interaction is strongly dependent on foulant and membrane properties (e.g., charge and hydrophobicity) (Liu et al. 2021a, Shan et al. 2016, Tang et al. 2011, Tang et al. 2009), a systematical investigation of their critical influences on colloidal fouling would be beneficial for membrane design and feedwater pretreatment.

In the current work, we report a collision-attachment (CA) approach (Liu et al. 2018) to relate the critical and limiting fluxes to metastable and long-term stable fluxes based on their dependence on initial permeate flux and colloid-membrane interaction. In CA model, fouling is recognized as two key processes, i.e., colloidal particles collision with the membrane and their subsequent attachment onto the membrane (Liu et al. 2021a, Liu et al. 2021b). In particular, the probability of successful colloidal attachment is described by Boltzmann equation, which can scale the critical roles of permeate flux and energy barrier of colloid-membrane on colloidal fouling (Liu et al. 2018). Although the CA model has been applied to explore the critical roles of permeate flux and energy barrier (Liu et al. 2021a, Liu et al. 2018, Liu et al. 2021b), the previous works rely on a highly simplified assumption of constant energy barrier of foulant-membrane with respect to filtration time. By incorporating the fouling transition behavior (i.e., from F-M to F-F), the CA approach developed herein can dissect the critical roles of permeate flux, $E_{f\text{-}m}$, and $E_{f\text{-}f}$ on colloidal stability. Unlike the existing publications that generally emphasized on raising the values of critical and limiting fluxes, this study highlights the critical roles of flux and energy barrier on period of stable flux. Furthermore, the crucial effects of membrane and foulant properties (i.e., charge and hydrophobicity) are also effectively evaluated through CA approach coupled with XDLVO theory. Our modelling results provide new insights and critical implications for fouling control under constant pressure mode.

2 Theory

In the subsections, the CA model is first presented in Sec. 2.1. Afterwards, the modifications of colloid-surface interaction and permeate flux are briefly introduced in Sec. 2.2 and Sec. 2.3, respectively.

2.1 Collision attachment model

The CA approach has been conventionally adopted to simulate the behavior of colloid-colloid collision in the field of coagulation (Thomas et al. 1999, Valioulis and List 1984). Liu and co-workers (Liu et al. 2021a, Liu et al. 2018) recently applied it to model membrane fouling behavior by recognizing a membrane as an infinitely large particle, and fouling as a series of collisions of colloidal particles with the membrane. As shown in Figure 1, colloidal particles can migrate towards the membrane and collide with the membrane under the permeate drag effect (Liu et al. 2018, Tang et al. 2009). According to CA model, the rate of fouling (i.e., rate of successful colloidal attachment onto the membrane, $\mathrm{d}m_f/\mathrm{d}t$) is determined by colloidal collision frequency JC_b and the corresponding attachment efficiency γ (Liu et al. 2018):

$$\frac{dm_f}{dt} = \gamma J C_b \tag{1}$$

where m_f is the mass of deposited colloidal particles in the filtration time t. J and C_b are the permeate flux and the colloidal concentration in bulk flow, respectively. The mass flux JC_b characterizes the frequency of colloidal particles colliding with the membrane, while the attachment efficiency γ represents the probability of colloidal attachment onto membrane for any collision event (Liu et al. 2021b). The value of γ can be further described by Boltzmann distribution law via considering the effects of hydrodynamics drag interaction, colloid-surface interaction as well as concentration polarization (CP) on colloidal deposition (Liu et al. 2018):

$$\gamma = \frac{1}{1 + \exp\left(\frac{\Delta E_b}{k_B T} - \frac{\Delta E_d}{k_B T} - \frac{J}{k_m}\right)} \tag{2}$$

where k_B is the Boltzmann's constant, and T is absolute temperature. ΔE_b is the energy barrier due to colloid-membrane interaction defending foulant attachment, the value of which is determined according to the modification of F-M to F-F interaction (see Sec. 2.2 for details). The term ΔE_d stands for the hydrodynamic drag interaction promoting colloidal attachment, and ΔE_d can be linked to the permeate flux through Stokes equation as (Liu et al. 2021b):

$$\Delta E_d = 3\pi\mu d_p J \times l_d = \beta J \tag{3}$$

where μ is the feed viscosity and d_p is the colloidal size. l_d is the relative displacement of colloid under drag force, with β the permeate drag coefficient.

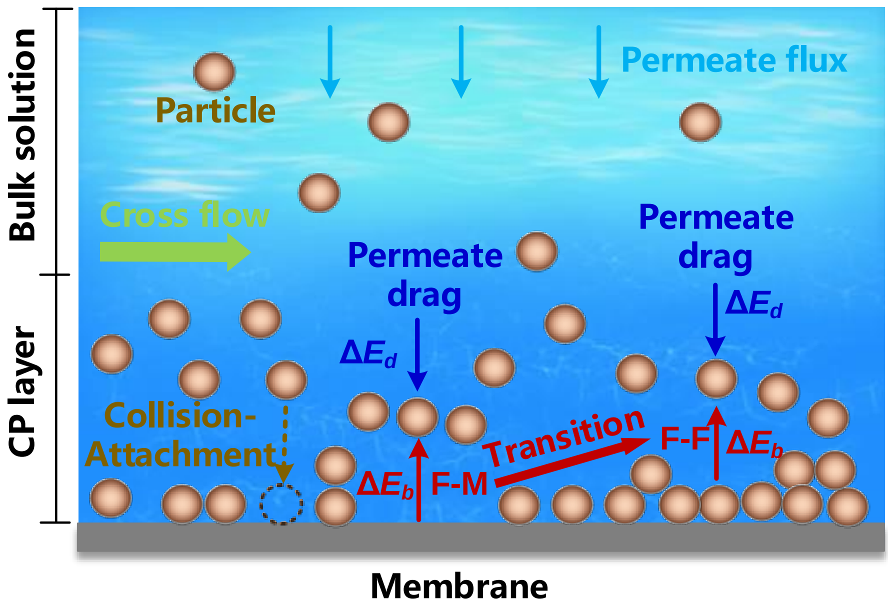

Figure 1 Schematics of colloidal transport and attachment in cross flow filtration

In Eq. 2, the term J/k_m accounts for the role of CP (i.e., the relative ratio of forward transport (J) over backward diffusion (k_m)), with k_m the mass transfer coefficient. In practice, k_m is often estimated based on Brownian diffusion coefficient D (Porter 1972) and the fluid channel geometry (Hoek et al. 2002). For a typical spacer-filled channel in crossflow filtration, k_m can be given by (Liu et al. 2021b):

$$k_m = 0.2\frac{u^{0.57}\rho^{0.17}D^{0.6}}{\mu^{0.17}d_h^{0.43}} \quad (4)$$

where u is the crossflow velocity and ρ is the fluid density. The term d_h is the hydrodynamic diameter of the membrane channel, the value of which can be calculated according to the spacer geometry (Liu et al. 2021b).

Overall, the terms $\Delta E_b/k_BT$, $\Delta E_d/k_BT$, and J/k_m in Eq. 2 incorporate the effects of energy barrier, permeate drag, and CP, respectively. Greater J gives rise to higher γ as a result of the raised drag and CP, whereas smaller γ appears at larger ΔE_b due to the enhanced colloid-membrane repulsion.

2.2 Colloid-surface interaction

As illustrated in Figure 1, when colloidal particles approach the membrane surface, the energy barrier ΔE_b arising from foulant – membrane interaction will resist their deposition, and those who overcome the energy barrier can successfully attach onto the membrane. The value of ΔE_b is determined by adopting a weighted average of F-M energy barrier ($E_{f\text{-}m}$) and F-F energy barrier ($E_{f\text{-}f}$) (Liu et al. 2020):

$$\Delta E_b = (1-\omega)E_{f-m} + \omega E_{f-f} \qquad (5)$$

where ω is the coverage coefficient to quantify the influence of deposited foulant and can be given by:

$$\omega = \frac{N_a}{N_c} = \frac{m_f}{m_c} \qquad 0 \le \omega \le 1 \qquad (6)$$

where N_a is the amount of colloidal particle number at time t, corresponding to the colloidal mass deposition m_f. N_c and m_c are the amount of respective particle number and particle mass required to fully cover the membrane surface, with m_c (in g/m^2) being approximately estimated by Liu et al. (2021a):

$$m_c = N_c \times m_p = \frac{A}{d_p^2} \times \frac{\rho_p \pi d_p^3}{6} = \frac{\rho_p \pi d_p}{6} \tag{7}$$

where m_p is the particle mass, ρ_p the particle density, and A the membrane unit area. Substituting Eqs. 6-7 into Eq. 5 can yield:

$$\Delta E_b = \left(1 - \frac{6m_f}{\rho_p \pi d_p}\right) E_{f-m} + \frac{6m_f}{\rho_p \pi d_p} E_{f-f} \qquad m_f \le \frac{\rho_p \pi d_p}{6} \tag{8a}$$

$$\Delta E_b = E_{f-f} \qquad m_f > \frac{\rho_p \pi d_p}{6} \tag{8b}$$

Eqs. 8 a, b can be used to determine the energy barrier ΔE_b as a function of deposited foulant mass m_f. The terms $E_{f\text{-}m}$ and $E_{f\text{-}f}$ in Eqs. 11 a, b can be calculated through XDLVO theory (Ding et al. 2013, Yin et al. 2020) based on the known colloidal and membrane properties (i.e., zeta potential and contact angle) (see Supporting information S2 for details).

2.3 Permeate flux equation

The foulant deposition can also modify the membrane flux under constant applied pressure. For any given time, the water flux can be determined according to membrane filtration equation (Hong and Elimelech 1997, Liu et al. 2020):

$$J = \frac{\Delta P}{\mu(R_m + \alpha_f \times m_f)} \quad (9)$$

where ΔP, R_m and m_f are the operating pressure, the membrane intrinsic resistance, and the mass of foulant deposition, respectively. It is worthwhile to note that since pore blocking is not involved in NF/RO, only cake filtration is the main behavior of colloidal fouling in our study. In this case, the cake resistance R_f can be generally given by the product of the specific cake resistance α_f and the amount of foulant mass deposition m_f (see Eq. 9). The value of α_f can be determined through Carmen–Kozeny equation (Carman 1997) or cake layer model (Tang et al. 2007). In this work, a referenced α_f of 3.0×10^{13} m/g is adopted for simulation based on our previous report (Liu et al. 2018).

The models in Sec. 2.1- Sec. 2.3 provide a facile way to investigate the critical roles of water flux, energy barrier of colloid-membrane interaction, and colloidal and membrane properties (zeta potential ζ and contact angle θ) on colloidal fouling. The detailed algorithm procedures are given in Supporting information S2. and model verifications indicate that the CA predicted water fluxes are in well agreement with the experimental results for colloidal fouling of NF membranes (refer to Supporting information S3 for details).

3 Results and discussion

3.1 Role of initial water flux

It has been well recognized that the critical flux J_C is affected by F-M energy barrier ($E_{f\text{-}m}$), while the limiting flux J_L is dominated by F-F energy barrier ($E_{f\text{-}f}$) (Liu et al. 2020, Tang and Leckie 2007). To comprehensively understand the relationship between J_C, J_L and metastable and long-term stable fluxes, we investigate the role of initial flux J_0 on colloidal stability under the conditions where $E_{f\text{-}m}$ equal to, less than, and greater than $E_{f\text{-}f}$, with the main simulation parameters listed in Table 1. At $E_{f\text{-}m}= E_{f\text{-}f}$ (12.0 k_BT), Figure 2a clearly shows that obvious flux decline occurs at great initial flux ($J_0 \geq 50$ μm/s), whereas water flux is still stable over the entire 100-h duration when $J_0 \leq 40$ μm/s. Therefore, the value of limiting flux is between 40 and 50 μm/s. A further close observation of the final pseudo-stable flux value for $J_0 = 50$ μm/s in Figure 2a suggests that the limiting flux should be around 45 μm/s. Such fouling phenomena fit the limiting flux theory (Tang and Leckie 2007) that permeate flux above J_L eventually approaches the J_L value (an estimated J_L of around 45 μm/s in Figure 2a). At the same time, our results also conform to the critical flux theory (Field et al. 1995): no fouling can be observed when initial flux below a critical value. As a result of the identical $E_{f\text{-}m}$ and $E_{f\text{-}f}$, the J_C and J_L share the same value accordingly.

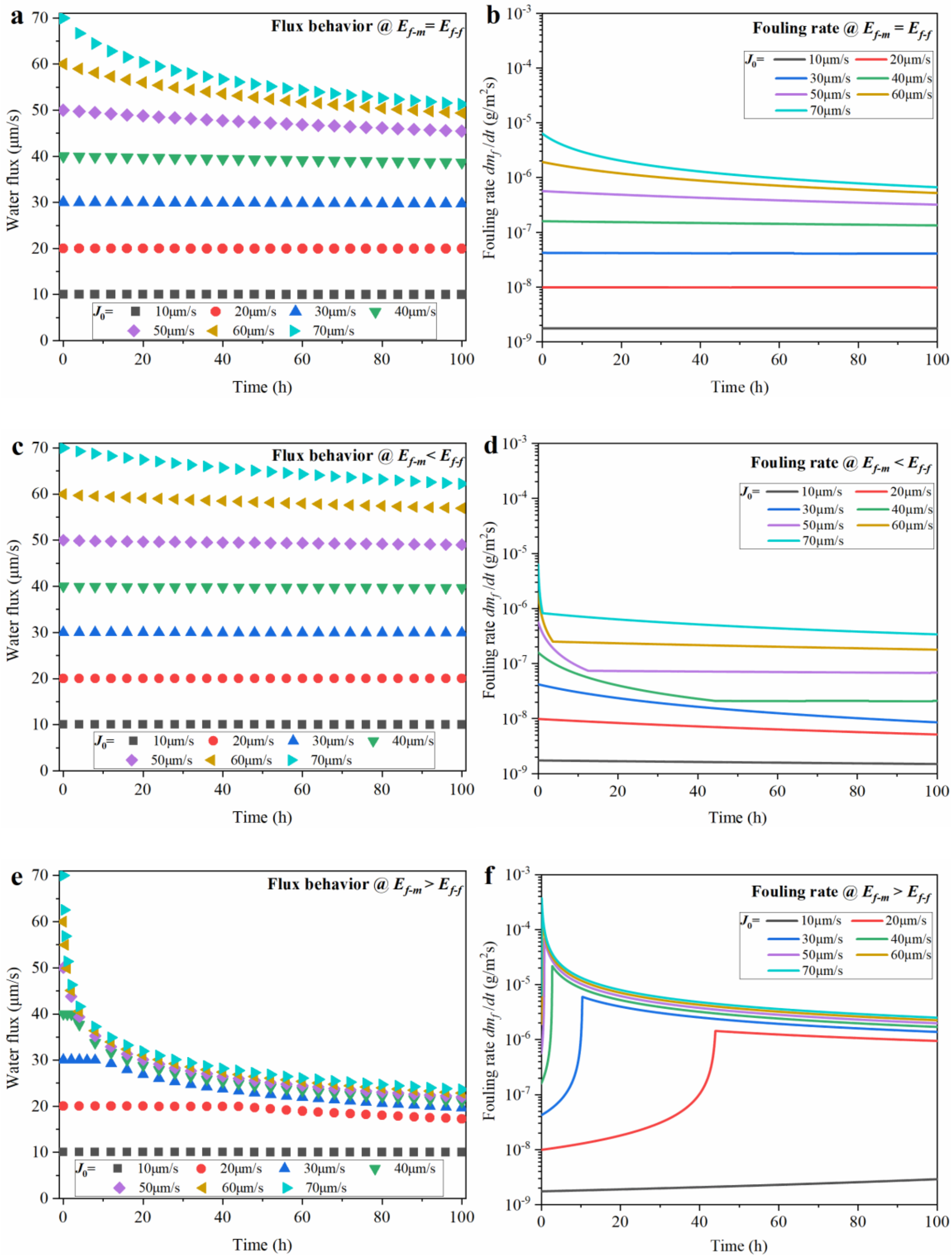

Figure 2 Effect of initial flux on flux behavior (left parts) and fouling rate (right parts) when (a, b) $E_{f\text{-}m}=E_{f\text{-}f}=12.0\ k_BT$, (c, d) $E_{f\text{-}m}=12.0\ k_BT$ & $E_{f\text{-}f}=14.0\ k_BT$, and (e, f) $E_{f\text{-}m}=12.0\ k_BT$ & $E_{f\text{-}f}=7.0\ k_BT$. See other simulation conditions in Table 1.

Table 1 Main parameters for modelling

	[a]Parameters	Value	Remarks
Feed characteristics	d_p	10 nm	Ref. (Liu et al. 2021a)
	C_b	10 mg/L	
	μ	8.9×10^{-4} Pa·s	Ref. (Liu et al. 2018)
Operation conditions	u	20 cm/s	Ref. (Liu et al. 2018)
	T	298 K	Ref. (Liu et al. 2018)
	J_0	1–100 μm/s	Ref. (Liu et al. 2018)
	R_m	4.50×10^{13} m^{-1}	Ref. (Liu et al. 2018)
	α_f	3.0×10^{13} m/g	Ref. (Liu et al. 2018)
Spacer Filaments	h_{sp}	1.12 mm	Note[a]
	d_{sp}	0.67 mm	Note[a]
	a_{sp}	3.05 mm	Note[a]
	θ_{sp}	90°	Note[a]
Mass transfer	k_B	1.38×10^{-23} J/K	
	D	4.91×10^{-11} m^2/s	Note[b]
	k_m	1.06×10^{-5} m/s	Eq. 4
Zeta potential	ζ_m	0 to −90 mV	Note[c]
	ζ_f	0 to −40 mV	Note[c]
Contact angle	θ_m	0° to 180°	Note[c]
	θ_f	0° to 180°	Note[c]
XDLVO theory	h_0	0.158 nm	Note[d]
	λ	0.6 nm	Note[d]
	$\varepsilon_\gamma\varepsilon_0$	6.94×10^{-10} F/m	Note[d]
	κ	0.104 nm^{-1}	Note[d]
Energy	β	$4.19 \times 10^{-9} \times d_p$	Ref. (Liu et al. 2018)
	k_BT	4.11×10^{-21} J	
	ΔE_b	0–20 k_BT	Note[d]

Notes: [a]The values of spacer thickness h_{sp}, filament diameter d_{sp}, mesh size a_{sp} and filaments intersection angle θ_{sp} are adopted according to a commercial spacer, and these parameters are used to calculate the hydrodynamic diameter of membrane channel. [b]The Brownian diffusion coefficient D can be determined through Stokes-Einstein relationship at known colloidal size d_p (Porter 1972). [c]The value ranges of membrane zeta potential ζ_m, foulant zeta potential ζ_f, membrane contact angle θ_m and foulant contact angle θ_f cover the typical membranes and colloids in RO and NF application. [d]The XDLVO parameters, i.e., minimum equilibrium separation distance (h_0 = 0.158 nm (Brant and Childress 2002)), decay length of AB interaction in water (λ = 0.6 nm

([Brant and Childress 2002]), dielectric permittivity of the solution ($\varepsilon_\gamma\varepsilon_0 = 6.94 \times 10^{-10}$ F/m (Brant and Childress 2002)), and inverse of the Debye screening length (κ=0.104 nm^{-1} at 1 mM NaCl solution (Lin et al. 2014)) are adopted to calculate the energy barriers of F-M and F-F (see Supporting information S2 for details). [e]The evolution of energy barrier over time is determined using a weighted average of the $E_{f\text{-}m}$ and $E_{f\text{-}f}$ based on the coverage of membrane surface by deposited foulants (refer to Sec. 2.2).

Essentially, the critical and limiting fluxes can be recognized as water flux corresponding to the negligible fouling rate. Under constant energy barrier ($E_{f\text{-}m} = E_{f\text{-}f}$), Figure 2b clearly shows an increasing J_0 from 10 to 70 μm/s results in an elevated initial dm_f/dt by orders of magnitude (i.e., from 10^{-9} to ~ 10^{-5} g/m^{2}s), reflecting the combined influences of increased collision frequency (Eq. 1), enhanced CP, and elevated attachment efficiency (Eq. 2). Over the entire 100-h filtration, a gradually decreased rate of fouling occurs for high J_0 ($\geq$ 50μm/s) whilst dm_f/dt remains constant at $J_0 \leq 40$ μm/s, with the latter corresponding to the sub-critical/limiting fluxes (Figure 2a). In view of critical/limiting flux being about 45μm/s in this set, the threshold dm_f/dt (i.e., the critical fouling rate below which little/no fouling happens) in this study should be in the range of about 2 ~ 5 ×10^{-7} g/m^{2}s, the value of which is comparable to our previous report (Liu et al. 2018).

Keeping $E_{f\text{-}m}$ at 12.0 k_BT but increasing $E_{f\text{-}f}$ to 14.0 k_BT brings about negligible flux declines during the whole 100-h filtration for J_0 of 50 and 60 μm/s, in addition to $J_0 \leq$ 40 μm/s (Figure 2c); the values of the former are above the critical flux (the J_C value should also be approximately 45 μm/s due to the fixed $E_{f\text{-}m}$). Although such results seem to be counter-intuitive, they can be reasonably interpreted by the evolutions of fouling rate and energy barrier. As shown in Figure 2d, despite that the fouling rates for $J_0 = 50$ and 60 μm/s are above the threshold dm_f/dt in the initial stage, their values become less than the threshold value only after a couple of hours, ensuring a relatively stable flux over the long-term filtration duration. Indeed, the initial attached colloidal particles can modify the membrane surface tending to a highly repulsive $E_{f\text{-}f}$ (Figure S2a of Supporting information S5) and thus lowering fouling rate substantially, eventually resulting in a self-terminated fouling behavior, even for the case of $E_{f\text{-}m} = 0$ (Supporting information S6). Our modelling supports the experimental observation (Wang and Tang 2011a) that for filtration of positively charged lysozyme by a negatively charged NF membrane, water flux can maintain a long-term stable state after initial slight loss, thanks to the strongly repulsive F−F interaction.

A much severe fouling happens at fixed $E_{f\text{-}m}$ (12.0 k_BT) but lowered $E_{f\text{-}f}$ (7.0 k_BT) (Figure 2e). At the end of 100-h filtration, all the fluxes for $J_0 \geq 20$ μm/s tend to a relatively low stable flux (<15 μm/s) due to the weak F-F interaction, revealing the limiting flux at such level. Our simulations underpin the previous reports (Tang et al. 2009, Tang and Leckie 2007): the long-term fouling is highly governed by F-F interaction. Nevertheless, owing to the strong F-M repulsion, there exists an initial metastable flux, with extended metastable period t_{mp} at decreased J_0. Specifically, rapid flux loss without metastable period is observed for high J_0 above 50 μm/s. Decreasing J_0 from 40 to 20 μm/s can effectively prolong the t_{mp} from only a couple hours to over 40 h. While for a low J_0 of

10 μm/s, the water flux remains stable without any obvious decline in the entire 100-h filtration. By comparison with the values of critical flux (J_C = ~45μm/s) and limiting flux (10 μm/s < J_L <15 μm/s), the metastable flux seems to be sub-critical flux but super-limiting flux. Despite being at sub-critical flux state, the substantial and continued flux declines occurs in the latter fouling period, which is against the typical critical flux theory that little fouling occurs when operational flux below a critical value (Bacchin et al. 2006). Nevertheless, it can be rationally explained by the fouling transition of colloid-surface interaction. Briefly, the conditioning of the membrane surface with initial attached particles will lower the energy barrier from relatively high $E_{f\text{-}m}$ toward weak $E_{f\text{-}f}$ (Figure S2b of Supporting information S5), serving as seeds for further foulant attachment, similar to the traditional nucleation to crystallization process (Le Gouellec and Elimelech 2002, Lin et al. 2005). Hence, although a high $E_{f\text{-}m}$ at sub-critical flux (J_0 =20-40 μm/s) indicates an excellent antifouling ability with negligible dm_f/dt (below threshold value), the "nucleus" effect of the deposited colloidal particles results in the accelerated rise of the fouling rate (above threshold value) (Figure 2f), eventually leading to the remarkable decline of water flux (Figure 2e). After the completion of transition from $E_{f\text{-}m}$ to $E_{f\text{-}f}$, the subsequent fouling rate begin to decline due to the decreased permeate drag at weak F-F domination.

Simulation results in Figures 2 a-f reveal that the role of initial flux is greatly affected by F-M and F-F interactions. According to the relative magnitudes of $E_{f\text{-}m}$ and $E_{f\text{-}f}$, the role of J_0 on stable flux can be summarized as the following three cases:

- $E_{f\text{-}m} = E_{f\text{-}f}$ (see Figure 3a). In the ideal condition that the energy barriers of F-M and F-F have the identical magnitude, the value of critical flux J_C is equal to that of limiting flux J_L. When J_0 is below J_C (or J_L), no flux decline occurs for long-term filtration. For J_0 above J_C (or J_L), the long-term stable flux value approaches the critical/limiting flux.
- $E_{f\text{-}m} < E_{f\text{-}f}$ (see Figure 3b). In this case, the critical flux J_C is less than the limiting flux J_L. When $J_0 \leq J_L$, flux for long-term filtration remains stable with negligible fouling even at J_0 above J_C, thanks to the conditioning of membrane surface by highly repulsive F-F interaction. While for $J_0 > J_L$, flux decline happens, and the long-term stable flux value achieves to J_L.
- $E_{f\text{-}m} > E_{f\text{-}f}$ (see Figure 3c, 3d). When the repulsion of F-M is greater than that of F-F, the value of J_C is above J_L. At $J_0 < J_L$, no flux reduction appears with J_0 value as the long-term stable flux. When J_0 above J_L but below J_C, the metastable flux (yellow curve in Figure 3c) appears as a result of high F-M repulsion, and its upper and lower limit are critical flux and limiting flux, respectively. The metastable flux period lasts longer at lower J_0, with a barely noticeable period at $J_0 = J_C$ but infinite period at $J_0 = J_L$ (Figure 3d). Nevertheless, owing to the "seed" effect of the initial attached foulant, the water flux will decrease to J_L value as the long-term stable flux (the green curve in Figure 3c). While for J_0 over J_C, water flux drops at the beginning of the filtration, and eventually approaches J_L for long-term filtration.

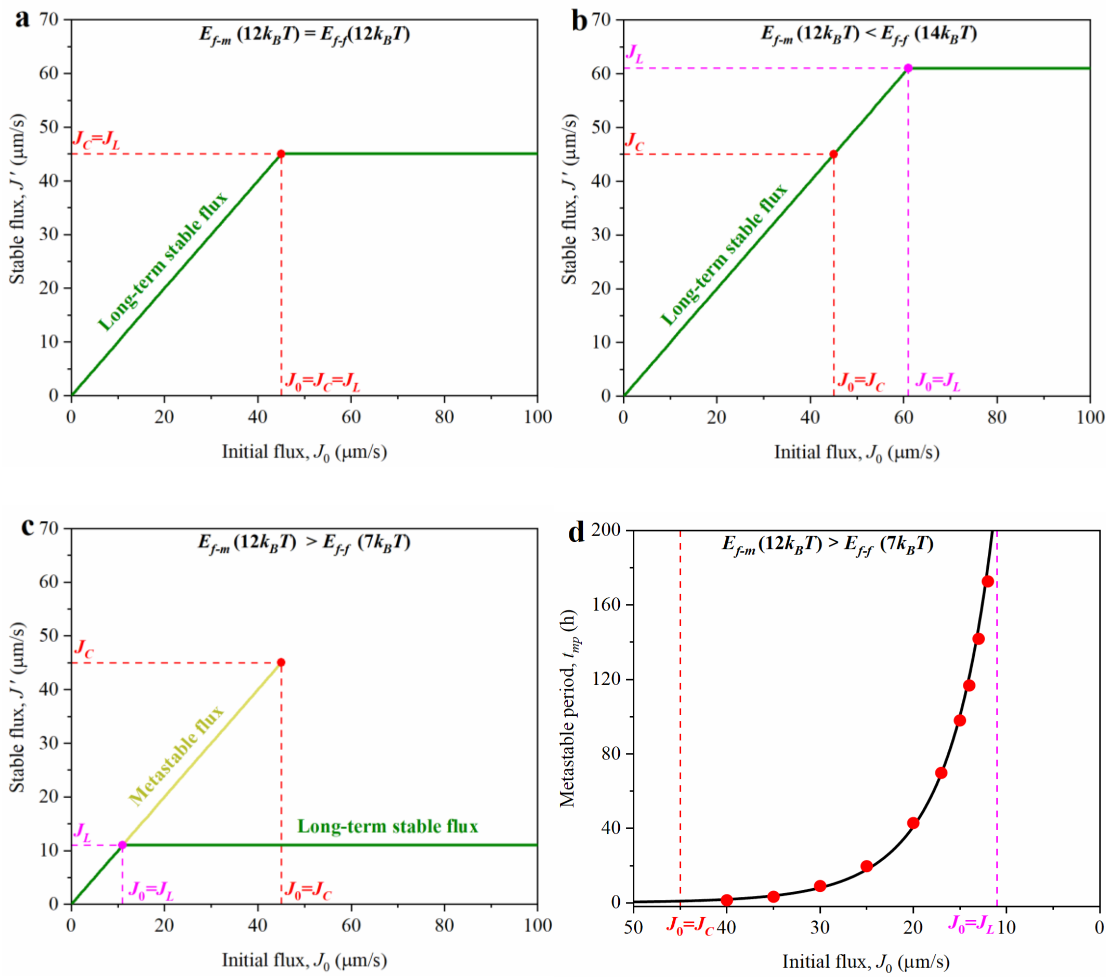

Figure 3 Effect of initial flux on stable flux at (a) $E_{f\text{-}m}$= $E_{f\text{-}f}$ =12.0 k_BT, (b) $E_{f\text{-}m}$=12.0 k_BT & $E_{f\text{-}f}$= 14.0 k_BT, and (c) $E_{f\text{-}m}$=12.0 k_BT & $E_{f\text{-}f}$ =7.0 k_BT, and (d) the metastable flux period. See other simulation conditions in Table 1. The metastable and long-term stable fluxes are determined based on the CA equations by adopting 3×10^{-7} g/m^{2}s as a threshold fouling rate dm_f/dt. In part (d), the scattered dots stand for the simulation results based on CA theory, with the curve fitted by a theoretical equation (See Supporting information S7 for details).

3.2 Role of membrane properties

Fouling can be greatly affected by membrane properties due to their important roles on foulant-membrane interaction (Hoek et al. 2003, Shan et al. 2016, Wang et al. 2019). For example, membranes with more hydrophilic surface generally exhibit better antifouling ability, thanks to the suppressed F-M hydrophobic attraction (Shan et al. 2016). To cater for the practical application, we dissect the crucial influence of membrane contact angle θ_m (standing for membrane hydrophilicity) on colloidal stability. At a long filtration time of 200 h, all the flux curves collapse to nearly the same pseudo-stable value (see Insert of Figure 4a), echoing the limiting flux independent of membrane properties. Despite that, our simulations clearly indicate that the initial flux behavior is highly dependent on membrane contact angle. With an initial flux of 20 μm/s, an extended metastable duration t_{mp} happens for membrane with smaller θ_m. Specifically, the metastable flux period is barely noticeable for $\theta_m > 60°$, while the t_{mp} can effectively be prolonged to ~ 5.0 and 55 h by decreasing θ_m to 56° and 55°, thanks to the enhanced hydrated repulsion of F-M at reduced θ_m (Figure 4c). Our simulations are consistent with the existing experimental observation of much longer stable-flux period (> 60 h) for a super-hydrophilic membrane, compared to the shorter metastable duration (< 1 h) for other less hydrophilic or more hydrophobic membranes (Shan et al. 2016).

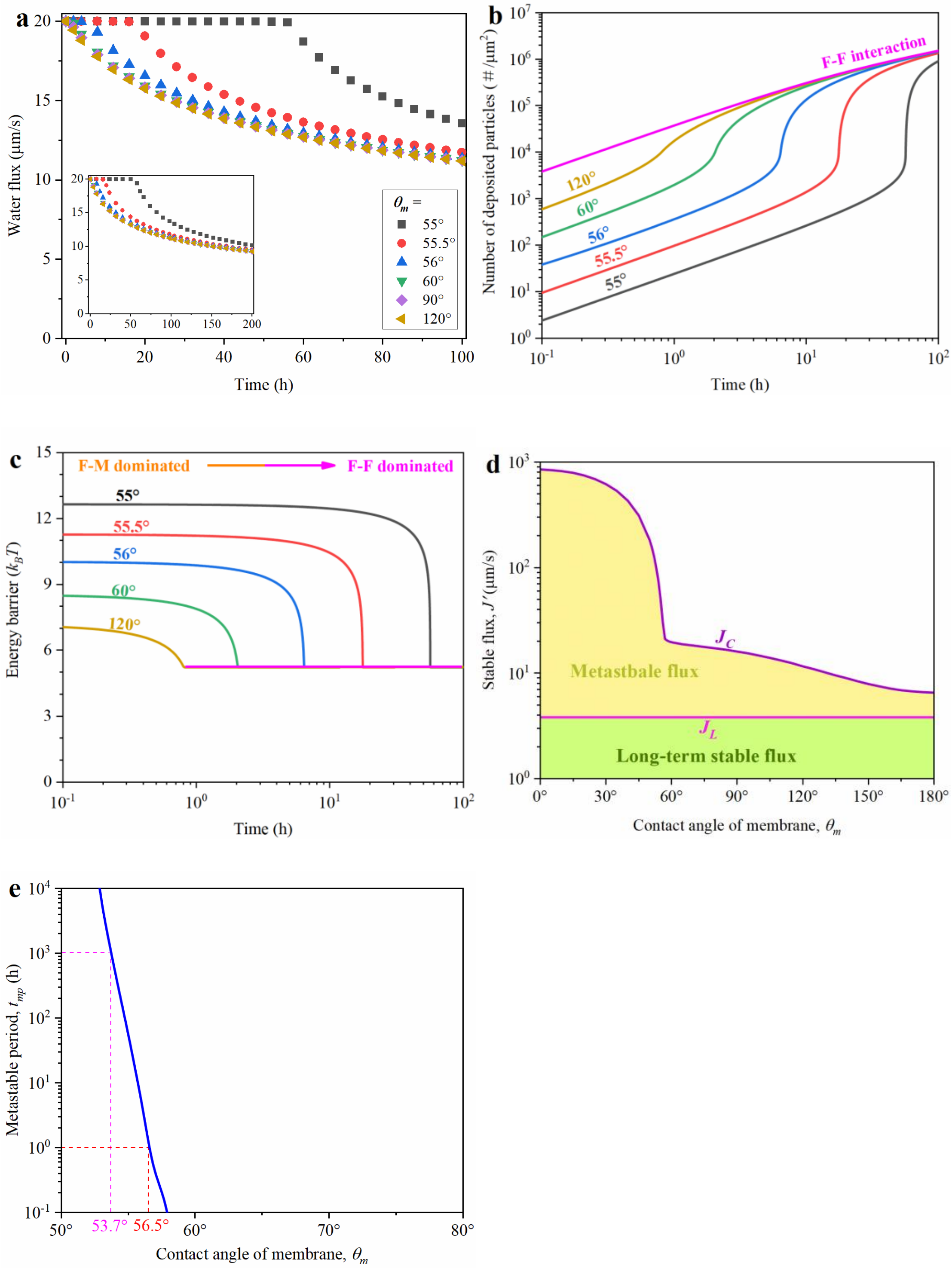

Figure 4 Effect of membrane contact angle θ_m on evolutions of (a) water flux, (b) particle deposition, (c) energy barrier, (d) stable flux, and (e) metastable period. The pink curve in part (b) is the evolution of particles accumulation dominated by F-F all the time. The stable fluxes and metastable periods in parts (d-e) are determined by

adopting 3×10^{-7} g/m^{2}s as a threshold fouling rate. The yellow and green shadings in part (d) represent the regions of metastable flux and long-term stable flux, respectively. Modelling conditions: θ_m = 0 - 180°, ζ_m= -60 mV, θ_f = 60°, ζ_f = -30 mV, J_0=20 µm/s (except part (d)), and the other simulation parameters listed in Table 1.

Figure 4b plots the evolution of particle deposition over time. In the initial filtration period, a slower foulant accumulation appears at lower contact angle as a result of smaller attachment efficiency (Eq. 2) arising from stronger F-M repulsion (Figure 4c). For each given θ_m, the number of deposited particles per square micrometer (#/µm^2) appears to be linearly dependent on filtration time on log scale, which is attributed to the nearly constant energy barrier in metastable duration (Figure 4c). However, once the initial deposited particles achieve a threshold amount, rapid foulant deposition happens, accompanied by remarkable barrier shifting from F-M to F-F (Figure 4c). Indeed, despite the initial particle deposition behaviors present distinct for membrane with different θ_m, their later fouling features are tending to the identical F-F dominated behavior (pink curve in Figure 4b).

Figure 4d further describes the effects of θ_m on stable flux. Briefly, the limiting flux value J_L is constant regardless of membrane properties, with the green shading (i.e., the sub-limiting fluxes) standing for the long-term stable flux region. While the critical flux J_C is strongly dependent on membrane θ_m, with higher J_C obtained at lower θ_m. An interesting observation in Figure 4d is that there seems to be a threshold θ_m around 56°. A slight decrease of θ_m by only several degrees can elevate J_C by more than one order of magnitudes, accompanied by the extremely expanding range of metastable fluxes (yellow shading in Figure 4d). Meanwhile, the metastable period t_{mp} is also greatly extended (Figure 4e). For example, the t_{mp} for J_0 of 20 μm/s is 1.0 h when θ_m at 56.5°, whereas it sharply increases 1000 time (i.e., 1000 h) when θ_m decrease to 53.7° ($\Delta\theta_m <$ 3.0°). Our results highlight the importance of tuning membrane contact angle below the threshold value for powerfully retarding fouling via raising the critical flux value and prolonging the metastable flux period effectively.

Similarly, the membrane zeta potential ζ_m also plays an important role on colloidal stability, where the larger critical flux and longer metastable period occur at decreased ζ_m with more negative charges (refer to Supporting information S8 for details). This result echoes a recent report (Wang et al. 2019) that more salient metastable flux period appears at increased application of external voltage, thanks to the strengthened electrostatic repulsion of F-M.

3.3 Role of colloidal properties

Like membrane properties, colloidal properties are equally important for fouling through the alteration of colloid-surface interaction (Liu et al. 2021a, Tang et al. 2011). As a typical example, rapid flux drops appeared at pH near the isoelectric point, high ionic strength, or high calcium ion, which is attributed to the suppressed F-M or F-F electrostatic repulsion (Tang et al. 2011, Tang et al. 2009). To better understand the vital influence of electrostatic interaction, Figure 5a investigates the effect of colloidal zeta potential on fouling development. Unlike the negligible influence of membrane properties on long-term fouling performance (Figure 4a), the colloidal zeta potential ζ_f is critical for fouling process from the beginning to end (Figure 5a). As shown in Figure

5a, flux decline is much milder over the entire filtration for foulant with more negative ζ_f, which is ascribed to their stronger F-M and F-F electrostatic repulsion (Figure 5b). Specifically, rapid flux declines without metastable period occur for colloid with slightly negative zeta potential (i.e., ζ_f = -10 and -20 mV). Decreasing ζ_f to -35 mV with more negative charge gives rise to a remarkable metastable flux period (t_{mp} ~20 h) followed by mild flux loss, as a result of the strengthened repulsion (Figure 5b) and thus reduced attachment probability (Eq. 2). Further reducing ζ_f to -40 mV leads to even long-term stable flux without obvious fouling, thanks to the domination of great energy barrier over the entire 100-h filtration (>12 k_BT, Figure 5b).

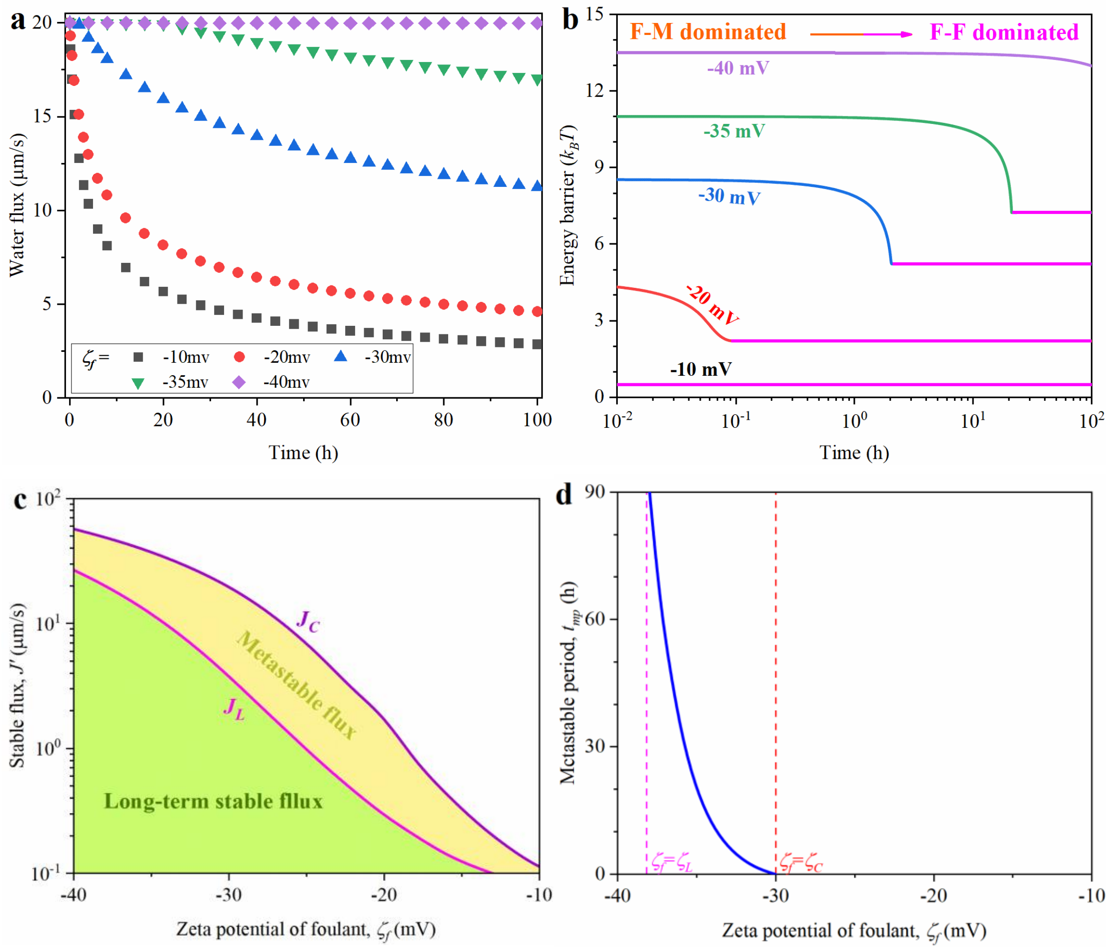

Figure 5 Effect of colloidal zeta potential ζ_f on the evolutions of (a) water flux, (b) energy barrier, (c) stable flux, and (d) metastable period. The stable fluxes and metastable periods in parts (c-d) are determined based on the CA equations by adopting 3×10^{-7} g/m^{2}s as a threshold fouling rate. The yellow and green shadings in part (c) represent the regions of metastable and long-term stable fluxes, respectively. In part (d), the starting and end of metastable period corresponds to the critical zeta potential ζ_C (-30mV) and limiting zeta potential ζ_L (-38 mV), the values of which are determined by considering initial flux (J_0 = 20 μm/s) as critical and limiting flux, respectively. Modelling conditions: ζ_f = 0 - 40 mV, θ_f = 60°, ζ_m= -60 mV, θ_m = 60°, J_0=20 μm/s (except part (c)), and the other simulation parameters listed in Table 1.

To fully disclose the key role of colloidal charge, Figure 5c draws the critical, limiting, metastable, and long-term stable fluxes as a function of ζ_f. Overall, a decreasing ζ_f from -10 to -40 mV with increasing negative charges leads to notably raised critical flux J_C and limiting flux J_L, i.e., from around ~ 0.1 to several dozen μm/s. Accordingly, the metastable flux values also go up more than two orders of magnitude (yellow shading in Figure 5c). At the same time, the metastable period t_{mp} becomes longer when ζ_f decreases from -30 to -40 mV at J_0 of 20 μm/s (Figure 5d). More importantly, like the membrane contact angle, there also exists a threshold colloidal ζ_f around -35 mV, in which a little bit reduction of ζ_f leads to orders of magnitude extension of metastable period t_{mp}. In addition to ζ_f, the colloidal contact angle θ_f also has significant influence on colloidal fouling, with less severe flux declines and longer metastable period occurring at decreased θ_f owing to the suppressed acid-base repulsion of colloid-membrane (refer to Supporting information S9 for details).

3.4 Interplay of flux and energy

Sec. 3.1 investigates the role of initial flux on colloidal fouling, while Secs. 3.2-3.3 dissect the effects of membrane and colloidal properties through their importance on F-M and F-F interaction. To achieve a comprehensive understanding of colloidal stability, the interplay of initial flux J_0 and energy barrier (i.e., $E_{f\text{-}m}$ and $E_{f\text{-}f}$) is further examined. In this section, we first define an initial threshold energy barrier E_{ith} (i.e., the critical energy barrier above which fouling is negligible for each given J_0). We then assess the joint role of flux - energy through comparing the magnitudes of E_{ith} to $E_{f\text{-}m}$ and $E_{f\text{-}f}$ (or J_0 to J_C and J_L). By adopting a threshold dm_f/dt of 3×10^{-7} g/m^{2}s, Figure 6a plots the curve of J_0 vs. E_{ith}. As expected, a higher J_0 requires a larger E_{ith} to lower attachment efficiency for avoiding fouling effectively. For instance, the value of E_{ith} is 8.6, 11.4 and 13.9 k_BT for J_0 of 20, 40, and 60 μm/s, respectively. Based on the relative magnitudes of E_{ith}, $E_{f\text{-}m}$ and $E_{f\text{-}f}$, the relations of critical, limiting fluxes to metastable and long-term stable fluxes are as follows (Figure 6b, c):

- Long-term stable flux region at $E_{ith} \leq E_{f\text{-}f}$ (see green shading at $J_0 \leq J_L$). Owing to the "self-terminated" fouling behavior for more repulsive F-F (compared to E_{ith}), little fouling happens, and membrane flux remains constant over a long-term filtration even for the case of $J_0 > J_C$.
- Unstable flux region at $E_{ith} > E_{f\text{-}f}$ & $E_{ith} > E_{f\text{-}m}$ (see red shading at $J_0 > J_L$ & $J_0 > J_C$). Since both barriers of F-M and F-F are too weak to effectively resist particle

deposition, obvious flux decline happens at the beginning of filtration, which is more severe at higher J_0 or lower $E_{f\text{-}m}$ or lower $E_{f\text{-}f}$ (marked by deeper red).

➢ Metastable flux region at $E_{f\text{-}f} < E_{ith} \leq E_{f\text{-}m}$ (see yellow shading at $J_L < J_0 \leq J_C$). In this region, the initial water flux can maintain stable due to the great $E_{f\text{-}m}$ ($\geq E_{ith}$), with longer metastable period appearing at smaller J_0 or greater $E_{f\text{-}m}$ or greater $E_{f\text{-}f}$ (indicated by deeper yellow). While the "nuclear" effect of the deposited particles leads to the rapid flux decline in the subsequent filtration by reducing the energy barrier towards weak $E_{f\text{-}f}$ ($<E_{ith}$). Eventually, the metastable flux degenerates to J_L as stable flux over the long-term filtration.

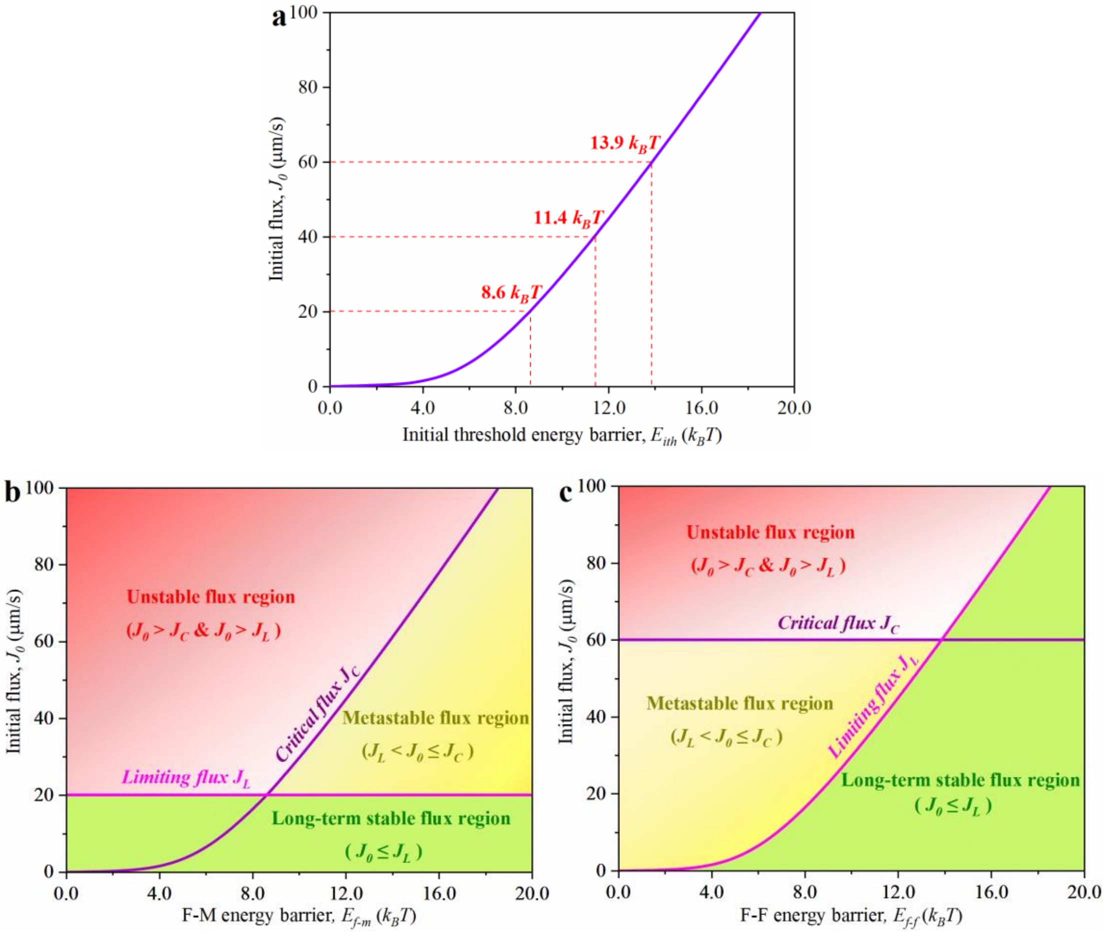

Figure 6 Relations of critical, limiting fluxes to metastable and long-term stable fluxes. (a) Initial flux J_0 versus initial threshold energy barrier E_{ith}; (b) Role of J_0 and $E_{f\text{-}m}$ at

fixed limiting flux (J_L= 20 μm/s); (c) Role of J_0 and $E_{f\text{-}f}$ at fixed critical flux (J_C= 60 μm/s). In parts (b-c), the purple and magenta curves are the critical flux and limiting flux, respectively; the green, yellow, and red shadings stand for the regions of long-term stable, initial unstable, and metastable fluxes, respectively, with a deeper yellow and red representing a longer metastable period and a faster flux decline, respectively. A threshold fouling rate dm_f/dt of 3×10^{-7} g/m^{2}s is adopted. Modelling conditions: J_0=0-100 μm/s, $E_{f\text{-}m}$=0 - 20 k_BT, $E_{f\text{-}f}$ =0 - 20 k_BT, with other parameters listed in Table 1.

Furthermore, Figure 7a provides more details for the joint effects of J_0 and $E_{f\text{-}m}$ on metastable flux period t_{mp}. For each given J_0, there seems to be a nearly linear increase of t_{mp} on $E_{f\text{-}m}$ at a log scale, with similar slopes for various J_0 (see the theoretical basis in Supporting information S7). For each fixed $E_{f\text{-}m}$, increased J_0 results in decreased metastable period obviously. However, when the energy difference between $E_{f\text{-}m}$ and E_{ith} as the horizontal coordinate, the role of initial flux becomes less discernible (Figure 7b), suggesting that the underlying factor in governing metastable period is the surplus of $E_{f\text{-}m}$ over E_{ith}.

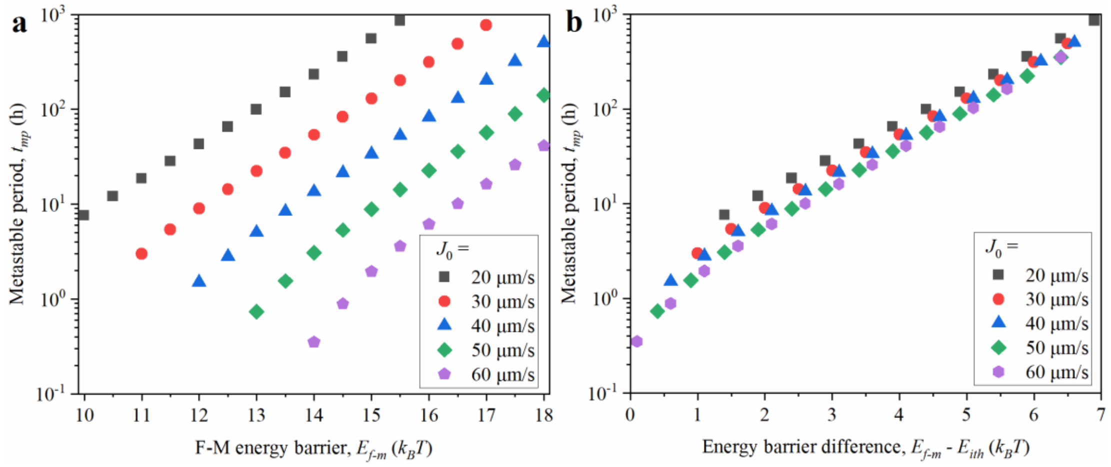

Figure 7 Effects of (a) F-M energy barrier $E_{f\text{-}m}$ and (b) energy barrier surplus of $E_{f\text{-}m}$ over E_{ith} on metastable period under initial flux ranging from 20 to 60 μm/s. A threshold

fouling rate of 3×10^{-7} g/m^{2}s is adopted. Modelling conditions: J_0=20-60 μm/s, $E_{f\text{-}m}$=10.0 -18.0 k_BT, $E_{f\text{-}f}$ =7.0 k_BT, with other simulation parameters listed in Table 1.

4 Conclusion and implications

For the first time, this work systematically investigates the relations of critical flux J_C and limiting flux J_L to metastable and long-term stable fluxes through a CA approach. Our simulations highlight the crucial roles of initial flux J_0, F-M energy barrier $E_{f\text{-}m}$, and F-F energy barrier $E_{f\text{-}f}$ on colloidal stability. When $J_0 \leq J_L$, the water flux remains stable over a long time even for the case of J_0 over J_C, thanks to the more repulsive $E_{f\text{-}f}$ compared to initial threshold energy barrier E_{ith} (i.e., the critical energy barrier above which no/little fouling occurs for each given J_0). At $J_0 > J_L$ & $J_0 > J_C$, water flux is unstable at the beginning of filtration owing to both weak $E_{f\text{-}m}$ ($<E_{ith}$) and $E_{f\text{-}f}$ ($<E_{ith}$), and the flux ultimately lowers to J_L as the long-term stable flux. Under the condition of $J_L < J_0 \leq J_C$, an initial metastable flux appears due to the high $E_{f\text{-}m}$ ($\geq E_{ith}$), with barely noticeable metastable period at J_0 = J_C but infinite period at J_0 decreasing to J_L. Furthermore, the metastable period can also be greatly prolonged at decreased contact angle or zeta potential of membrane or foulant. Nevertheless, rapid flux decline occurs subsequently owing to the energy barrier shifting to weak $E_{f\text{-}f}$ ($<E_{ith}$), and the metastable flux eventually degenerates to J_L as the long-term stable flux.

Our results have significant implications for regulating operational conditions. When adopting critical flux J_C and limiting flux J_L as fouling control strategies, one needs to distinguish the short-term stable (i.e., metastable) and long-term stable flux. The long-term stable flux is independent of critical flux but dependent on limiting flux, whereas the metastable flux is dependent on both critical flux and limiting flux. Sub-critical flux operation may lead to a short-term stable flux if J_0 above J_L, owing to the "seed" effect of the initial deposited foulants. To ensure a long-term stable flux, the operational flux J_0 should be below J_L. In real application, the operating flux selection is highly dependent on energy barriers of F-M and F-F. In the context of $E_{f\text{-}m}=E_{f\text{-}f}$, controlling water flux below critical/limiting flux should be a great guide for fouling control. While at high $E_{f\text{-}m}$ but low $E_{f\text{-}f}$, critical flux should be adopted as the upper bound of operating flux for fouling control. For the case of small $E_{f\text{-}m}$ but great $E_{f\text{-}f}$, limiting flux (J_L) should be applied as the upper limit of operation flux for fouling control.

Since unstable flux happens at water flux over both critical flux and limiting flux, high operating flux J_0 above J_C and J_L should be strictly avoided due to the great permeate drag that promotes severe fouling, which can significantly affect membrane operational stability. However, excessive pursuit of low flux ($J_0 << J_C$ or $J_0 << J_L$) is also not recommended as lowered water production means increased investment and operational cost. Due to the trade-off effect between metastable flux value and its period (Figure 3d), moderate flux is often adopted (e.g., 12–45 L m^{-2} h^{-1} for brackish water treatment) in practice (Greenlee et al. 2009). Besides, operating flux selection should also consider the types of membrane module in real application. For typical NF/RO spiral-wound module applied in desalination or water reuse, owing to the difficult membrane cleaning, a relatively lower J_0 is favored to achieve longer metastable duration. While for hollow fiber membranes (or flat sheet membranes) with effectively cleaning, a relatively larger J_0 (still below J_C) within tolerable cleaning frequency can be implemented to obtain more productive water.

Modelling results also have important guidelines for membrane preparation and feedwater adjustment. For coping with unfavorable feed (small $E_{f\text{-}f}$ and low J_L values), the design of membranes with more hydrophilic or more charged is fundamentally essential for achieving higher critical flux and longer metastable period (see Figure 4 and Supporting information S8). Furthermore, membrane selection should be in accordance with the anticipated operating flux J_0 (or a demand water production). As suggested in Figure 7, the underlying factor in governing metastable flux period is the surplus of F-M energy barrier $E_{f\text{-}m}$ over the initial threshold energy barrier E_{ith} (i.e., the critical energy barrier above which fouling is negligible for each given J_0). Therefore, the $E_{f\text{-}m}$ value for selected NF/RO membranes should be far more than E_{ith} to achieve a relatively long metastable period. However, it should be clearly aware that even the excellent antifouling membrane may fail due to the energy barrier shifting to weak repulsive F−F. Considering the great influences of colloidal properties on both $E_{f\text{-}m}$ and $E_{f\text{-}f}$, pretreatment problematic feedwater (e.g., via coagulation (Wang et al. 2020), adsorption (Zhang et al. 2023), and oxidation (Zhang et al. 2022)) may be an effective way to reduce fouling for long-term filtration. As enlightened from Figure 5 and

Supporting information S9, adjusting contact angle and zeta potential of colloids in accordance with the threshold value is able to resist fouling powerfully through effectively raising the J_C and J_L values. More importantly, a high J_L can ensure a high value of long-term stable flux due to the self-terminated fouling behavior even for poor antifouling membranes (Supporting information S6).

Traditionally, flux–pressure experimental observations (Fradin and Field 1999, Wu et al. 1999) were adopted to determine a steady state flux (i.e., critical flux). However, the duration of the fouling test using this method was often performed within a couple of hours (e.g., < 2h), and thus the obtained pseudo-stable flux may not maintain over a long-time filtration owing to the fouling shifting from high $E_{f\text{-}m}$ to low $E_{f\text{-}f}$ repulsion. Compared to the flux-pressure measurements, the CA approach developed herein provides a facile approach for not only determining the value of stable flux (i.e., J_C and J_L), but also predicting the period of metastable flux.

Acknowledgements

This study was financially supported by the Special Project for Research and Development in Key areas of Guangdong Province (2022B0101090004), the Basic and Applied Basic Research Foundation of Guangdong Province (2020A1515110833, and 2021A0505110013) and National Natural Science Foundation of China (42107431 and 51708130).

References

Aimar, P. and Field, R. (1992) Limiting flux in membrane separations: A model based on the viscosity dependency of the mass transfer coefficient. Chemical Engineering Science 47(3), 579-586.

Bacchin, P., Aimar, P. and Field, R.W. (2006) Critical and sustainable fluxes: Theory, experiments and applications. Journal of Membrane Science 281(1-2), 42-69.

Bacchin, P., Aimar, P. and Sanchez, V. (1995) Model for colloidal fouling of membranes. AIChE Journal 41(2), 368-376.

Boussu, K., Belpaire, A., Volodin, A., Van Haesendonck, C., Van der Meeren, P., Vandecasteele, C. and Van der Bruggen, B. (2007) Influence of membrane and colloid characteristics on fouling of nanofiltration membranes. Journal of Membrane Science 289(1-2), 220-230.

Brant, J.A. and Childress, A.E. (2002) Assessing short-range membrane–colloid interactions using surface energetics. Journal of Membrane Science 203(1), 257-273.

Carman, P.C. (1997) Fluid flow through granular beds. Chemical Engineering Research and Design 75, S32-S48.

Chen, Y.F., Liu, C., Setiawan, L., Wang, Y.N., Hu, X. and Wang, R. (2017) Enhancing pressure retarded osmosis performance with low-pressure nanofiltration pretreatment: Membrane fouling analysis and mitigation. Journal of Membrane Science 543, 114-122.

Ding, Y., Tian, Y., Li, Z., Wang, H. and Chen, L. (2013) Interaction energy evaluation of the role of solution chemistry and organic foulant composition on polysaccharide fouling of microfiltration membrane bioreactors. Chemical Engineering Science 104(Supplement C), 1028-1035.

Etemadi, H., Amirjangi, A., Ghasemian, N. and Shokri, E. (2020) Synthesis and characterization of polycarbonate/TiO_2 ultrafiltration membranes: Critical flux determination. Chemical Engineering & Technology 43(11), 2247-2258.

Field, R., Wu, D., Howell, J. and Gupta, B. (1995) Critical flux concept for microfiltration fouling. Journal of Membrane Science 100(3), 259-272.

Field, R.W. and Pearce, G.K. (2011) Critical, sustainable and threshold fluxes for membrane filtration with water industry applications. Advances in Colloid and Interface Science 164(1-2), 38-44.

Fradin, B. and Field, R.W. (1999) Crossflow microfiltration of magnesium hydroxide suspensions: determination of critical fluxes, measurement and modelling of fouling. Separation and Purification Technology 16(1), 25-45.

Greenlee, L.F., Lawler, D.F., Freeman, B.D., Marrot, B. and Moulin, P. (2009) Reverse osmosis desalination: Water sources, technology, and today's challenges. Water Research 43(9), 2317-2348.

Hoek, E.M.V., Bhattacharjee, S. and Elimelech, M. (2003) Effect of membrane surface roughness on colloid−membrane DLVO interactions. Langmuir 19(11), 4836-4847.

Hoek, E.M.V., Kim, A.S. and Elimelech, M. (2002) Influence of crossflow membrane filter geometry and shear rate on colloidal fouling in reverse osmosis and nanofiltration separations. Environmental Engineering Science 19(6), 357.

Hong, S. and Elimelech, M. (1997) Chemical and physical aspects of natural organic matter (NOM) fouling of nanofiltration membranes. Journal of Membrane Science 132(2), 159-181.

Khanzada, N.K., Farid, M.U., Kharraz, J.A., Choi, J., Tang, C.Y., Nghiem, L.D., Jang, A. and An, A.K. (2020) Removal of organic micropollutants using advanced membrane-based water and wastewater treatment: A review. Journal of Membrane Science 598, 117672.

Lan, Y., Groenen-Serrano, K., Coetsier, C. and Causserand, C. (2017) Fouling control using critical, threshold and limiting fluxes concepts for cross-flow NF of a complex matrix: Membrane bioreactor effluent. Journal of Membrane Science 524, 288-298.

Le Gouellec, Y.A. and Elimelech, M. (2002) Calcium sulfate (gypsum) scaling in nanofiltration of agricultural drainage water. Journal of Membrane Science 205(1-2), 279-291.

Lin, C.J., Shirazi, S. and Rao, P. (2005) Mechanistic model for $CaSO_4$ fouling on nanofiltration membrane. Journal of Environmental Engineering 131(10), 1387-1392.

Lin, T., Lu, Z. and Chen, W. (2014) Interaction mechanisms and predictions on membrane fouling in an ultrafiltration system, using the XDLVO approach. Journal of Membrane Science 461, 49-58.

Liu, J., Fan, Y., Sun, Y., Wang, Z., Zhao, D., Li, T., Dong, B. and Tang, C.Y. (2021a) Modelling the critical roles of zeta potential and contact angle on colloidal fouling with a coupled XDLVO - collision attachment approach. Journal of Membrane Science 623, 119048.

Liu, J., Huang, T., Ji, R., Wang, Z., Tang, C.Y. and Leckie, J.O. (2020) Stochastic collision-attachment-based Monte Carlo simulation of colloidal fouling: Transition from foulant-clean-membrane interaction to foulant-fouled-membrane interaction. Environmental Science & Technology 54(19), 12703-12712.

Liu, J., Wang, Z., Tang, C.Y. and Leckie, J.O. (2018) Modeling dynamics of colloidal fouling of RO/NF membranes with a novel collision-attachment approach. Environmental Science & Technology 52(3), 1471-1478.

Liu, J., Zhao, Y., Fan, Y., Yang, H., Wang, Z., Chen, Y. and Tang, C.Y. (2021b) Dissect the role of particle size through collision-attachment simulations for colloidal fouling of RO/NF membranes. Journal of Membrane Science 638, 119679.

Osorio, S.C., Biesheuvel, P.M., Spruijt, E., Dykstra, J.E. and van der Wal, A. (2022) Modeling micropollutant removal by nanofiltration and reverse osmosis membranes: Considerations and challenges. Water Research 225, 119130.

Porter, M.C. (1972) Concentration polarization with membrane ultrafiltration. Industrial & Engineering Chemistry Product Research and Development 11(3), 234-248.

Shan, L., Fan, H., Guo, H., Ji, S. and Zhang, G. (2016) Natural organic matter fouling behaviors on superwetting nanofiltration membranes. Water Research 93, 121-132.

Shannon, M.A., Bohn, P.W., Elimelech, M., Georgiadis, J.G., Mariñas, B.J. and Mayes, A.M. (2008) Science and technology for water purification in the coming decades. Nature 452(7185), 301-310.

Su, Z.Y., Liu, T., Li, X., Graham, N. and Yu, W.Z. (2021) Beneficial impacts of natural biopolymers during surface water purification by membrane nanofiltration. Water Research 201, 117330.

Tang, C.Y., Chong, T.H. and Fane, A.G. (2011) Colloidal interactions and fouling of NF and RO membranes: A review. Advances in Colloid and Interface Science 164(1-2), 126-143.

Tang, C.Y., Kwon, Y.-N. and Leckie, J.O. (2007) Characterization of humic acid Fouled reverse osmosis and nanofiltration membranes by transmission electron microscopy and streaming potential measurements. Environmental Science & Technology 41(3), 942-949.

Tang, C.Y., Kwon, Y.N. and Leckie, J.O. (2009) The role of foulant–foulant electrostatic interaction on limiting flux for RO and NF membranes during humic acid fouling—Theoretical basis, experimental evidence, and AFM interaction force measurement. Journal of Membrane Science 326(2), 526-532.

Tang, C.Y. and Leckie, J.O. (2007) Membrane independent limiting flux for RO and

NF membranes fouled by humic acid. Environmental Science & Technology 41(13), 4767-4773.

Thomas, D., Judd, S. and Fawcett, N. (1999) Flocculation modelling: a review. Water Research 33(7), 1579-1592.

Valioulis, I.A. and List, E.J. (1984) Collision efficiencies of diffusing spherical particles: hydrodynamic, van der Waals and electrostatic forces. Advances in Colloid and Interface Science 20(1), 1-20.

Wang, J., Wang, L., Miao, R., Lv, Y., Wang, X., Meng, X., Yang, R. and Zhang, X. (2016) Enhanced gypsum scaling by organic fouling layer on nanofiltration membrane: Characteristics and mechanisms. Water Research 91, 203-213.

Wang, K., Xu, L., Li, K., Liu, L., Zhang, Y. and Wang, J. (2019) Development of polyaniline conductive membrane for electrically enhanced membrane fouling mitigation. Journal of Membrane Science 570-571, 371-379.

Wang, P.P., Wang, F.H., Jiang, H.C., Zhang, Y.C., Zhao, M., Xiong, R.H. and Ma, J. (2020) Strong improvement of nanofiltration performance on micropollutant removal and reduction of membrane fouling by hydrolyzed-aluminum nanoparticles. Water Research 175, 119130.

Wang, Y.-N. and Tang, C.Y. (2011a) Fouling of nanofiltration, reverse osmosis, and ultrafiltration membranes by protein mixtures: the role of inter-foulant-species interaction. Environmental Science & Technology 45(15), 6373-6379.

Wang, Y.-N. and Tang, C.Y. (2011b) Protein fouling of nanofiltration, reverse osmosis, and ultrafiltration membranes—The role of hydrodynamic conditions, solution chemistry, and membrane properties. Journal of Membrane Science 376(1), 275-282.

Wu, D.X., Howell, J.A. and Field, R.W. (1999) Critical flux measurement for model colloids. Journal of Membrane Science 152(1), 89-98.

Xie, W., Li, J., Sun, F., Dong, W. and Dong, Z. (2021) Strategy study of critical flux/threshold flux on alleviating protein fouling of PVDF-TiO_2 modified membrane. Journal of Environmental Chemical Engineering 9(5), 106148.

Yin, Z.Q., Ma, Y.Q., Tanis-Kanbur, B. and Chew, J.W. (2020) Fouling behavior of colloidal particles in organic solvent ultrafiltration. Journal of Membrane Science 599, 106148.

Zhang, J., Yu, S., Wang, J., Zhao, Z.-P. and Cai, W. (2023) Advanced water treatment process by simultaneous coupling granular activated carbon (GAC) and powdered carbon with ultrafiltration: Role of GAC particle shape and powdered carbon type. Water Research 231, 119606.

Zhang, L., Graham, N., Kimura, K., Li, G.B. and Yu, W.Z. (2022) Targeting membrane fouling with low dose oxidant in drinking water treatment: Beneficial effect and biological mechanism. Water Research 209, 117953.

Zhang, R., Liu, Y., He, M., Su, Y., Zhao, X., Elimelech, M. and Jiang, Z. (2016) Antifouling membranes for sustainable water purification: Strategies and mechanisms. Chemical Society Reviews 45(21), 5888-5924.

781

Graphic Abstract

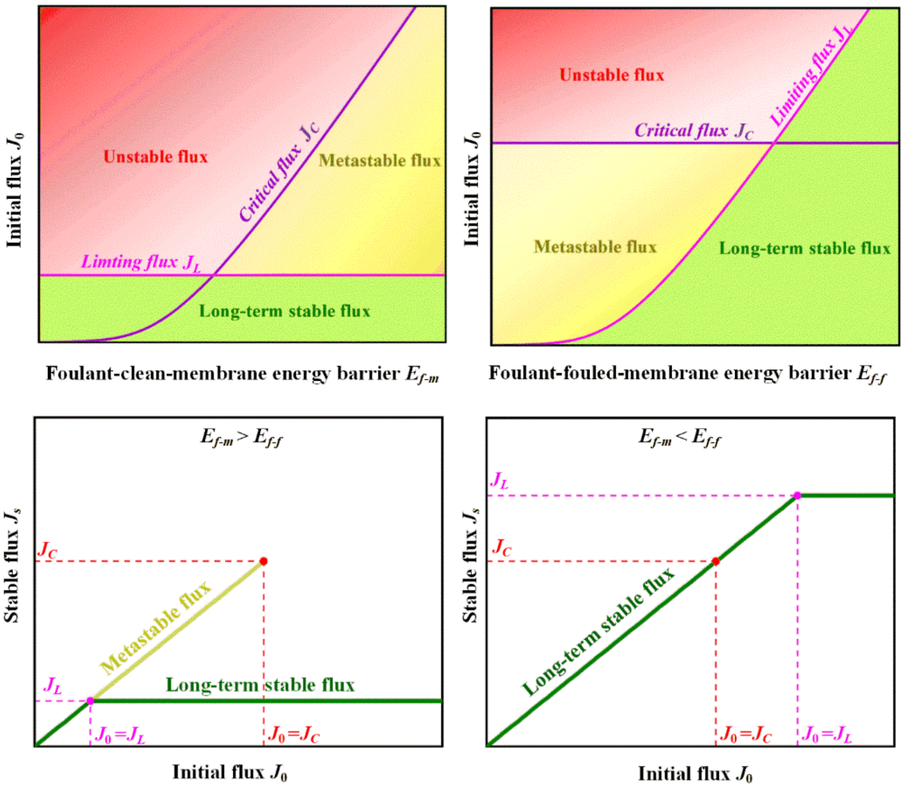

Table 1 Main parameters for modelling

	[a]Parameters	Value	Remarks
Feed characteristics	d_p	10 nm	Ref. (Liu et al. 2021a)
	C_b	10 mg/L	
	μ	8.9×10^{-4} Pa·s	Ref. (Liu et al. 2018)
Operation conditions	u	20 cm/s	Ref. (Liu et al. 2018)
	T	298 K	Ref. (Liu et al. 2018)
	J_0	1–100 μm/s	Ref. (Liu et al. 2018)
	R_m	4.50×10^{13} m^{-1}	Ref. (Liu et al. 2018)
	α_f	3.0×10^{13} m/g	Ref. (Liu et al. 2018)
Spacer Filaments	h_{sp}	1.12 mm	Note[a]
	d_{sp}	0.67 mm	Note[a]
	a_{sp}	3.05 mm	Note[a]
	θ_{sp}	90°	Note[a]
Mass transfer	k_B	1.38×10^{-23} J/K	
	D	4.91×10^{-11} m^2/s	Note[b]
	k_m	1.06×10^{-5} m/s	Eq. 4
Zeta potential	ζ_m	0 to −90 mV	Note[c]
	ζ_f	0 to −40 mV	Note[c]
Contact angle	θ_m	0° to 180°	Note[c]
	θ_f	0° to 180°	Note[c]
XDLVO theory	h_0	0.158 nm	Note[d]
	λ	0.6 nm	Note[d]
	$\varepsilon_\gamma \varepsilon_0$	6.94×10^{-10} F/m	Note[d]
	κ	0.104 nm^{-1}	Note[d]
Energy	β	$4.19 \times 10^{-9} \times d_p$	Ref. (Liu et al. 2018)
	k_BT	4.11×10^{-21} J	
	ΔE_b	0–20 k_BT	Note[d]

Notes: [a]The values of spacer thickness h_{sp}, filament diameter d_{sp}, mesh size a_{sp} and filaments intersection angle θ_{sp} are adopted according to a commercial spacer, and these parameters are used to calculate the hydrodynamic diameter of membrane channel. [b]The Brownian diffusion coefficient D can be determined through Stokes-Einstein relationship at known colloidal size d_p (Porter 1972). [c]The value ranges of membrane zeta potential ζ_m, foulant zeta potential ζ_f, membrane contact angle θ_m and foulant contact angle θ_f cover the typical membranes and colloids in RO and NF application. [d]The XDLVO parameters, i.e., minimum equilibrium separation distance (h_0 = 0.158 nm (Brant and Childress 2002)), decay length of AB interaction in water (λ = 0.6 nm

(Brant and Childress 2002)), dielectric permittivity of the solution ($\varepsilon_{\gamma}\varepsilon_{0}$ = 6.94 × 10^{-10} F/m (Brant and Childress 2002)), and inverse of the Debye screening length (κ=0.104 nm^{-1} at 1 mM NaCl solution (Lin et al. 2014)) are adopted to calculate the energy barriers of F-M and F-F (see Supporting information S2 for details). [e]The evolution of energy barrier over time is determined using a weighted average of the $E_{f\text{-}m}$ and $E_{f\text{-}f}$ based on the coverage of membrane surface by deposited foulants (refer to Sec. 2.2).

Figure 1

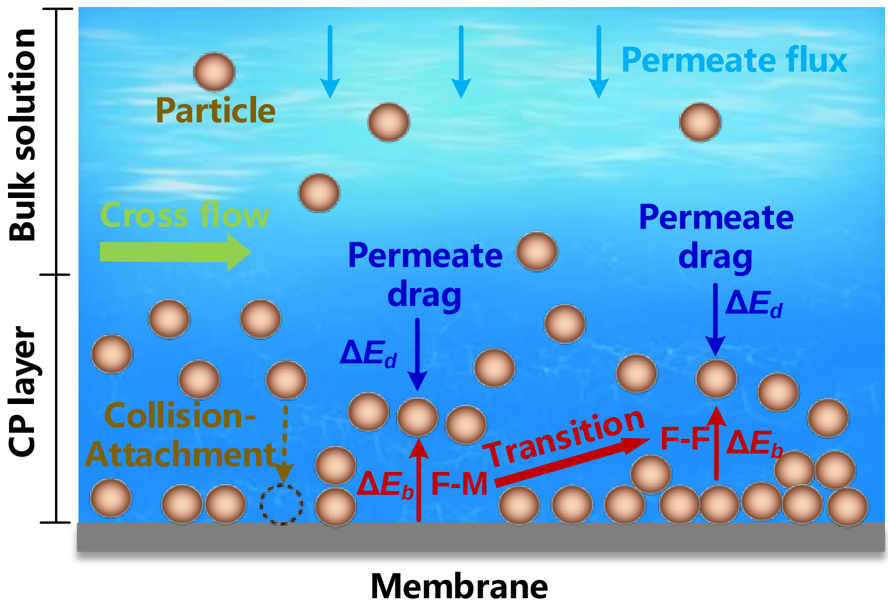

Figure 1 Schematics of colloidal transport and attachment in cross flow filtration

Figure 2

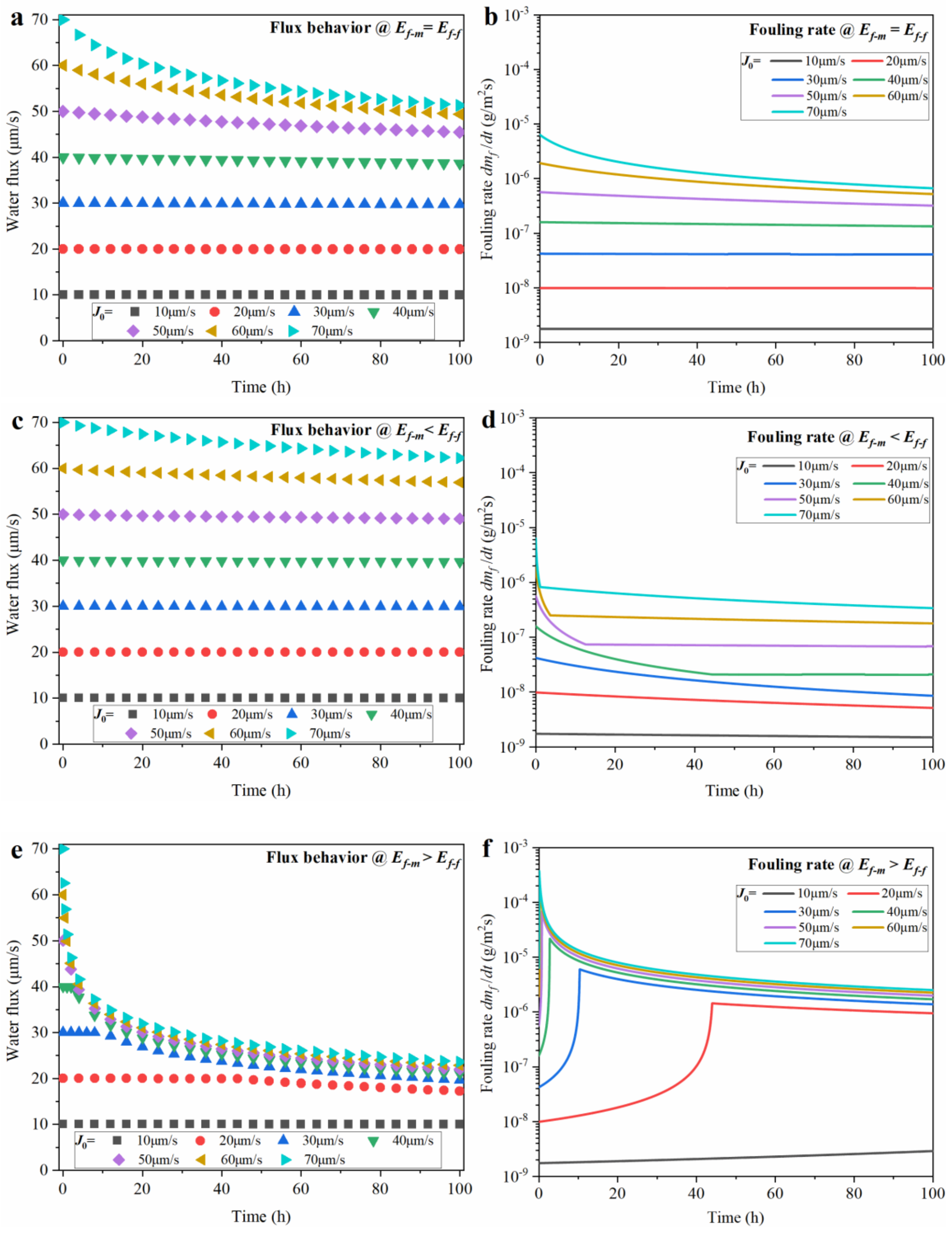

Figure 2 Effect of initial flux on flux behavior (left parts) and fouling rate (right parts) when (a, b) $E_{f\text{-}m}=E_{f\text{-}f}=12.0\ k_BT$, (c, d) $E_{f\text{-}m}=12.0\ k_BT$ & $E_{f\text{-}f}=14.0\ k_BT$, and (e, f) $E_{f\text{-}m}=12.0\ k_BT$ & $E_{f\text{-}f}=7.0\ k_BT$. See other simulation conditions in Table 1.

Figure 3

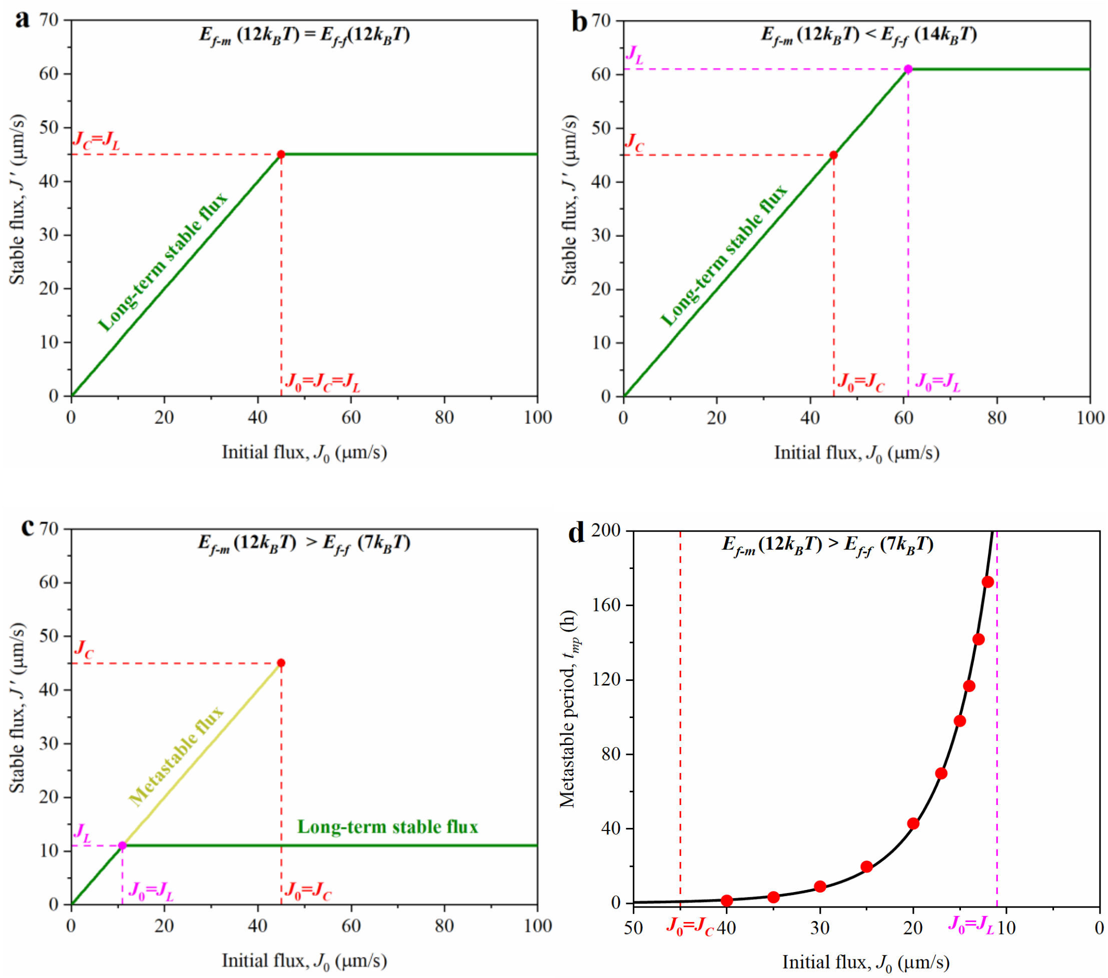

Figure 3 Effect of initial flux on stable flux at (a) $E_{f\text{-}m}$= $E_{f\text{-}f}$ =12.0 k_BT, (b) $E_{f\text{-}m}$=12.0 k_BT & $E_{f\text{-}f}$= 14.0 k_BT, and (c) $E_{f\text{-}m}$=12.0 k_BT & $E_{f\text{-}f}$ =7.0 k_BT, and (d) the metastable flux period. See other simulation conditions in Table 1. The metastable and long-term stable fluxes are determined based on the CA equations by adopting 3×10^{-7} g/m^{2}s as a threshold fouling rate dm_f/dt. In part (d), the scattered dots stand for the simulation results based on CA theory, with the curve fitted by a theoretical equation (See Supporting information S7 for details).

Figure 4

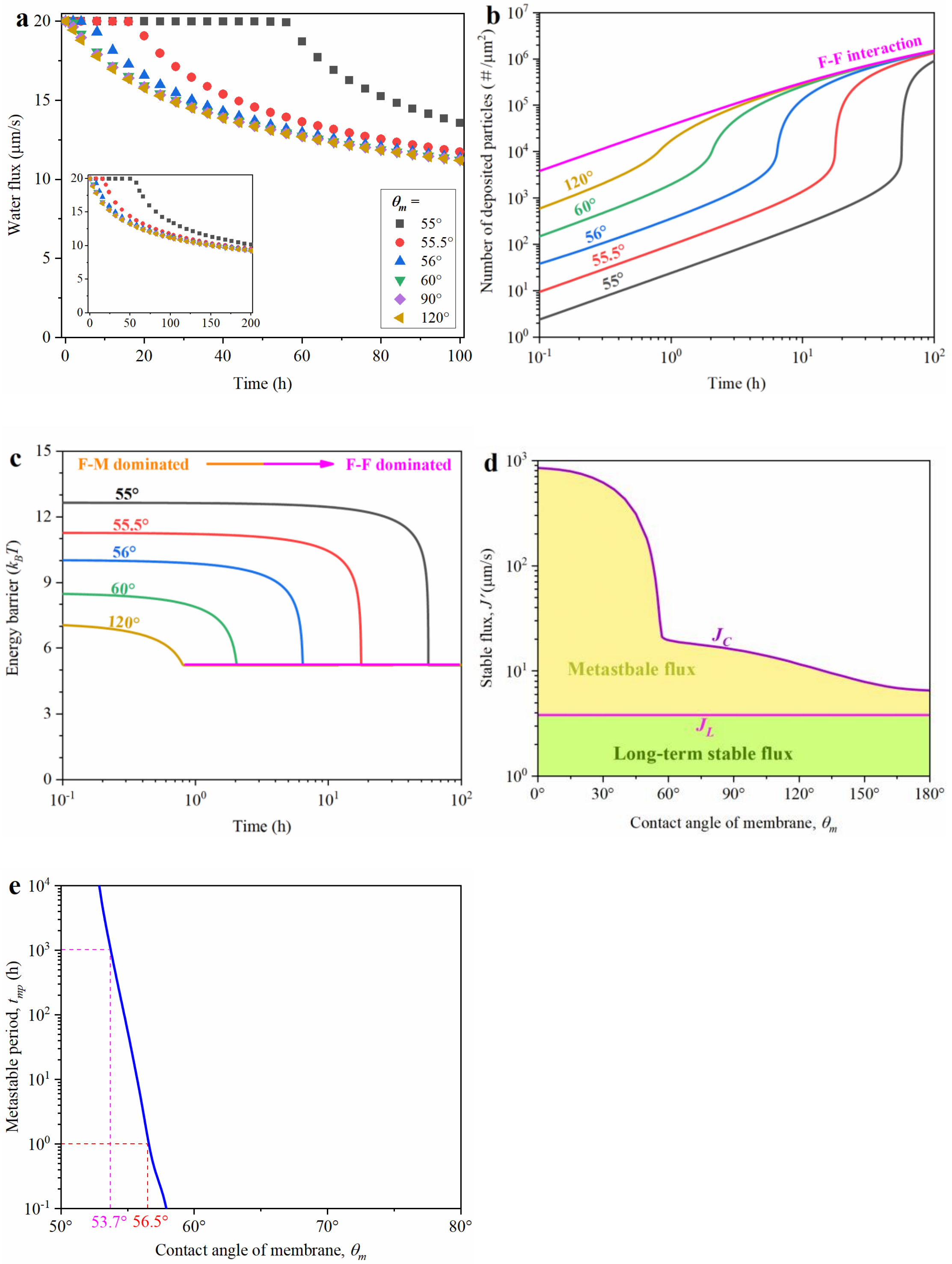

Figure 4 Effect of membrane contact angle θ_m on evolutions of (a) water flux, (b) particle deposition, (c) energy barrier, (d) stable flux, and (e) metastable period. The pink curve in part (b) is the evolution of particles accumulation dominated by F-F all the time. The stable fluxes and metastable periods in parts (d-e) are determined by

adopting 3×10^{-7} g/m^{2}s as a threshold fouling rate. The yellow and green shadings in part (d) represent the regions of metastable flux and long-term stable flux, respectively. Modelling conditions: θ_m = 0 - 180°, ζ_m= -60 mV, θ_f = 60°, ζ_f = -30 mV, J_0=20 μm/s (except part (d)), and the other simulation parameters listed in Table 1.

Figure 5

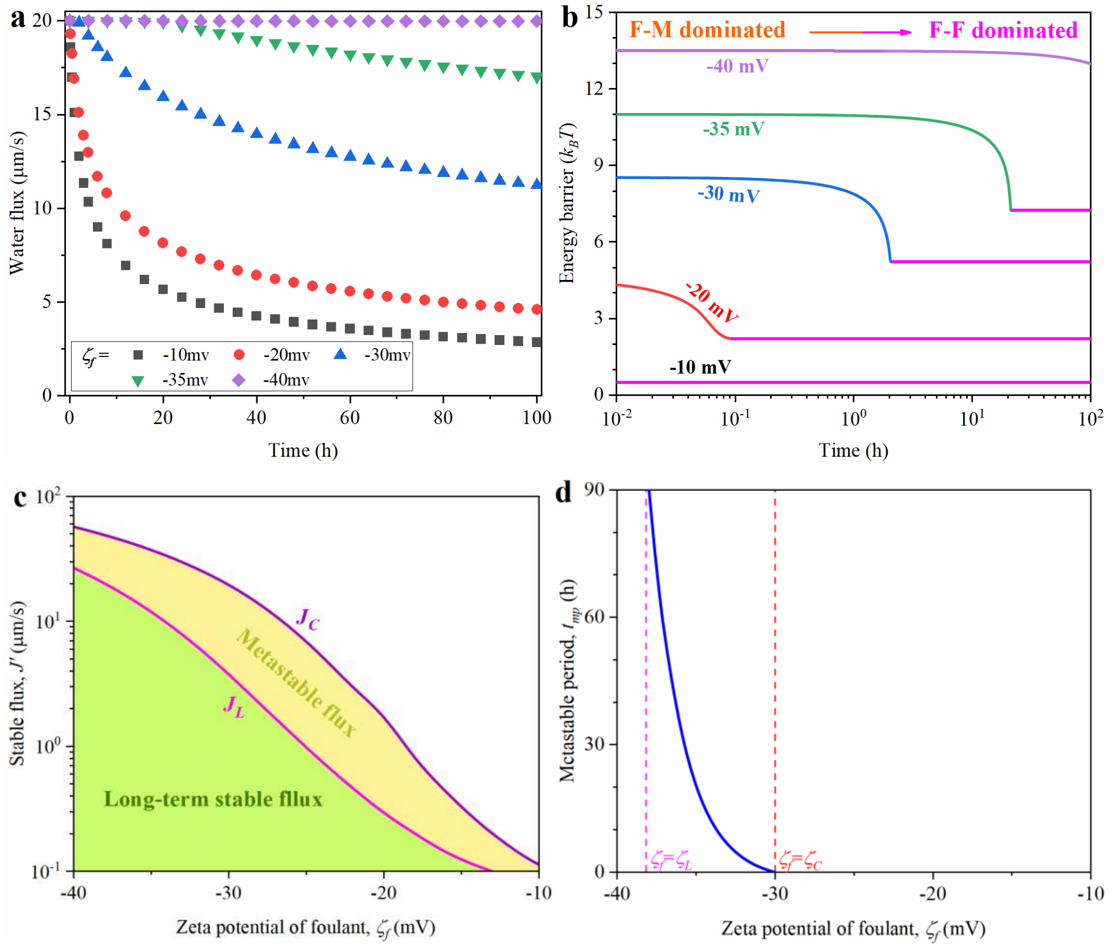

Figure 5 Effect of colloidal zeta potential ζ_f on the evolutions of (a) water flux, (b) energy barrier, (c) stable flux, and (d) metastable period. The stable fluxes and metastable periods in parts (c-d) are determined based on the CA equations by adopting 3×10^{-7} g/m^{2}s as a threshold fouling rate. The yellow and green shadings in part (c) represent the regions of metastable and long-term stable fluxes, respectively. In part (d), the starting and end of metastable period corresponds to the critical zeta potential ζ_C (-30mV) and limiting zeta potential ζ_L (-38 mV), the values of which are determined by considering initial flux (J_0 = 20 μm/s) as critical and limiting flux, respectively. Modelling conditions: ζ_f = 0 - 40 mV, θ_f = 60°, ζ_m= -60 mV, θ_m = 60°, J_0=20 μm/s (except part (c)), and the other simulation parameters listed in Table 1.

Figure 6

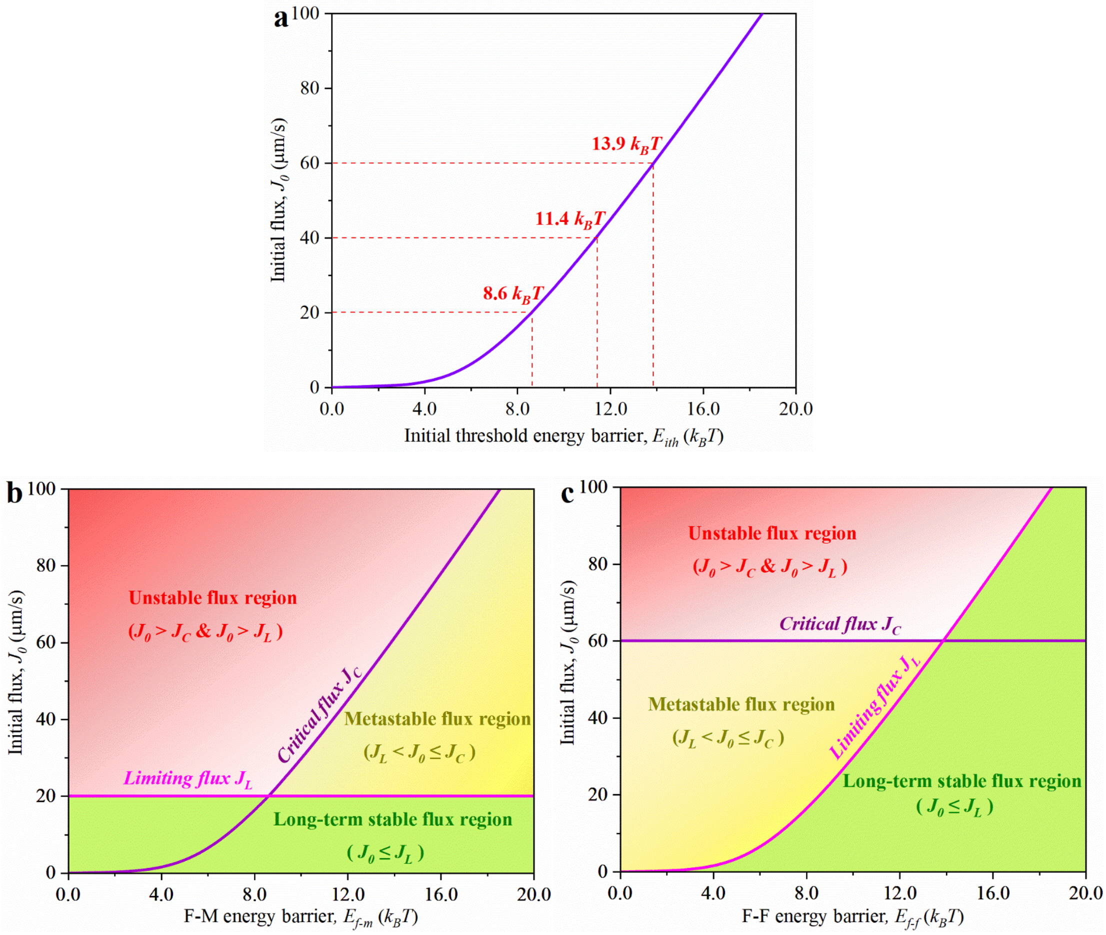

Figure 6 Relations of critical, limiting fluxes to metastable and long-term stable fluxes. (a) Initial flux J_0 versus initial threshold energy barrier E_{ith}; (b) Role of J_0 and $E_{f\text{-}m}$ at fixed limiting flux (J_L= 20 µm/s); (c) Role of J_0 and $E_{f\text{-}f}$ at fixed critical flux (J_C= 60 µm/s). In parts (b-c), the purple and magenta curves are the critical flux and limiting flux, respectively; the green, yellow, and red shadings stand for the regions of long-term stable, initial unstable, and metastable fluxes, respectively, with a deeper yellow and red representing a longer metastable period and a faster flux decline, respectively. A threshold fouling rate dm_f/dt of 3×10^{-7} g/m^{2}s is adopted. Modelling conditions: J_0=0-100 µm/s, $E_{f\text{-}m}$=0 - 20 k_BT, $E_{f\text{-}f}$ =0 - 20 k_BT, with other parameters listed in Table 1.

Figure 7

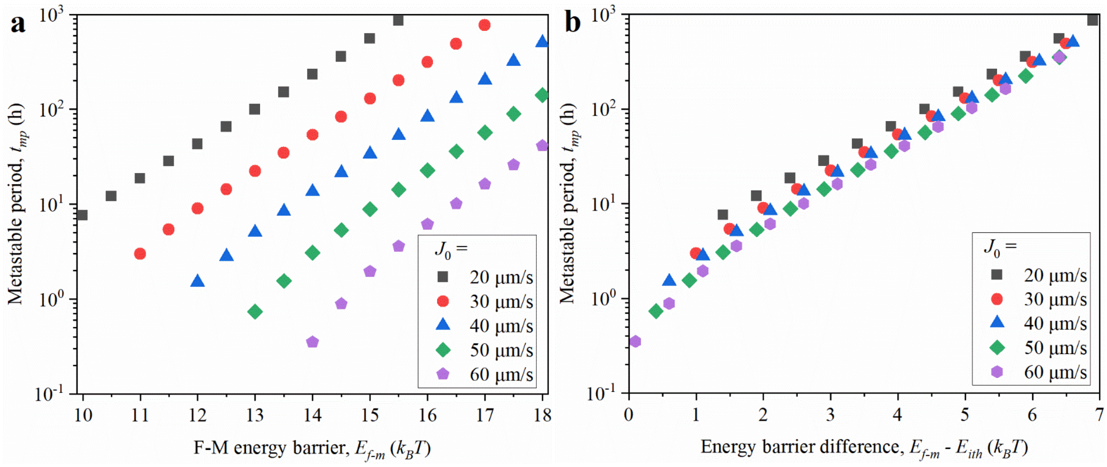

Figure 7 Effects of (a) F-M energy barrier $E_{f\text{-}m}$ and (b) energy barrier surplus of $E_{f\text{-}m}$ over E_{ith} on metastable period under initial flux ranging from 20 to 60 μm/s. A threshold fouling rate of 3×10^{-7} g/m^{2}s is adopted. Modelling conditions: J_0=20-60 μm/s, $E_{f\text{-}m}$=10.0 -18.0 k_BT, $E_{f\text{-}f}$ =7.0 k_BT, with other simulation parameters listed in Table 1.